ELSEVIER

Journal of Fluids and Structures 23 (2007) 809–838

JOURNAL OF FLUIDS AND STRUCTURES

www.elsevier.com/locate/jfs

Oscillation of shallow flow past a cavity: Resonant coupling with a gravity wave

A. Ekmekci, D. Rockwell*

Department of Mechanical Engineering and Mechanics, 356 Packard Laboratory, 19 Memorial Drive West, Lehigh University, Bethlehem, PA 18015, USA

Received 8 February 2006; accepted 18 December 2006
Available online 23 April 2007

Abstract

Self-excited oscillations of flow past a cavity are generated in a shallow free-surface system. The shear layer past the cavity opening has two basic forms: a separated free-shear flow; and a shear flow along a slotted plate. Instabilities of these classes of shear flows can couple with the fundamental gravity-wave mode of the adjacent cavity. The dimensionless frequencies of both types of oscillations scale on the length of the cavity opening, rather than the gap distance between the slats, i.e., a large-scale instability is always prevalent. A technique of high-image-density particle image velocimetry allows acquisition and interpretation of global, instantaneous images of the flow pattern, including patterns of vorticity and Reynolds stress correlation. Use of a cinema approach provides representations of the timewise evolution of the global, instantaneous flow structure, and thereby definition of the amplitude peaks and phase angles of the coupled fluctuations via auto- and cross-spectral techniques. These methods, along with global, averaged representations of the fluctuating flow field, provide insight into the onset of fully coupled (phase-locked) oscillations of the shear flow past the resonator cavity. The common, as well as the distinctive, features of the resonant-coupled instability of the shear flow past the slotted plate are characterized, relative to the corresponding coupled instability of the free-shear layer. Varying degrees of resonant coupling between the unstable shear layer and the adjacent resonator are attained by variations of the inflow velocity, which yield changes of the predominant oscillation frequency, relative to the resonant frequency of the adjacent cavity. Well-defined, coherent oscillations are indeed attainable for the case of the shear flow along the slotted plate, though their amplitude is significantly mitigated relative to the case of a free-shear layer. The degree of organization of the self-excited, resonant-coupled oscillation and the manner in which it varies with open area ratio and geometry of the plate are interpreted in terms of the flow structure on either side of, and within, the slotted plate; these features are compared with the corresponding structure of the free-shear layer oscillations.

Keywords: Cavity oscillations; Gravity wave resonance

1. Introduction

An unstable shear layer past an opening of finite length can give rise to coherent, self-sustaining oscillations. In the event that the shear layer is bounded by a resonant cavity, i.e., a cavity with acoustic or free-surface resonant modes

*Corresponding author. Tel.: +1 610 758 4107; fax: +1 610 758 6224.
E-mail address: dor0@lehigh.edu (D. Rockwell).

0889-9746/$ - see front matter © 2007 Elsevier Ltd. All rights reserved.
doi:10.1016/j.jfluidstructs.2006.12.005

tuned with those of the unstable shear layer, coupled oscillations can occur, giving rise to flow-induced noise and vibration. Corresponding applications occur in a wide variety of external flow systems, such as along the fuselage of an aircraft and the hull of a marine vessel, or in internal flow systems, involving junctions of pipe systems and valves of large-scale pipes and power plants. In the event that the flow is along a perforated surface bounded by a cavity, as opposed to the free-shear situation in the aforementioned configurations, resonant-coupled instabilities within each of the holes of the perforation can give rise to "singing", as well as generation of broadband noise. Corresponding applications include surface treatments along the walls of aircraft engines and silencers in compressor and ventilation systems, as well as within exhaust mufflers in automobiles.

In the following, previous related investigations of fundamental features of these configurations are briefly reviewed.

1.1. Self-sustained oscillations of an impinging free-shear flow in absence of a resonant coupling

If a flow system is purely hydrodynamic, that is, a resonant mode of an acoustic or gravity wave does not exist, occurrence of organized, self-sustained oscillations is attainable for a wide range of configurations, including, for example, jet-edge and a rectangular cavity. The central elements associated with these oscillations, which incorporate a feedback mechanism, are described in the early investigation of Powell (1961) and subsequently by DeMetz and Farabee (1977), Rockwell and Naudascher (1978, 1979), Rockwell (1983), Blake (1986), Gharib and Roshko (1987), Chomaz et al. (1988), Crighton (1992), Burroughs and Stinebring (1994), Howe (1997, 1998), Rockwell (1998), Kwon (1998), Ziada (1999), Kuo and Huang (2001) and Rowley et al. (2002). In essence, the onset of an instability in the separated shear layer instigates the oscillation, which acts in concert with an upstream influence resulting from the shear layer instability-impingement edge interaction, to yield coherent oscillations. Techniques for control of these oscillations, as well as issues associated with higher speeds, are described and assessed by Cattafesta et al. (2003).

1.2. Self-excited free-shear layer oscillations coupled with an acoustic resonator

If the unstable shear layer described in the previous section couples with an acoustic mode of an adjacent resonator, particularly pronounced oscillations can occur. Rockwell and Naudascher (1978), Blake (1986), Howe (1998) and Rockwell et al. (2003) summarize extensive investigations of locked-on flow past cavity configurations, including not only quasi-two-dimensional geometries, but also circular and triangular configurations. Howe (1975, 1980) provides a generalized conceptual framework for this class of resonant-coupled oscillations. Representative configurations include jet excitation of a long (closed) organ pipe, as addressed by Cremer and Ising (1967) and Fletcher (1979); jet-sequential orifice plates addressed by Flatau and Van Moorham (1990), Hourigan et al. (1990), and Huang and Weaver (1991); the wake from a flat plate in a test-section, characterized originally by Parker (1966) and subsequently by Cumpsty and Whitehead (1971) and Stoneman et al. (1988); a cavity shear layer-cavity resonator, characterized by DeMetz and Farabee (1977), Elder (1978) and Nelson et al. (1981, 1983); a cavity shear layer-side branch duct/pipe, investigated by Bruggeman (1987), Bruggeman et al. (1989, 1991), Ziada and Bühlmann (1992), Kriesels et al. (1995), Hofmans (1998), and Dequand et al. (2003); a cavity shear layer-Helmholtz resonator pursued by Dequand et al. (2003) and Dequand et al. (2003); and a cavity shear layer-long pipeline pursued by Davies (1981, 1996), Rockwell and Schachenmann (1982, 1983), Rockwell et al. (2003), Geveci et al. (2003), and Oshkai et al. (2004).

1.3. Self-excited oscillations of a shear flow past a perforated/slotted plate coupled with an acoustic resonator

Flow past a perforated surface can give rise to unstable shear layer oscillations, which involve small-scale vortex formation in each of the holes of a perforated surface or plate. Such instabilities can couple with either a Helmholtz or standing wave resonant mode of a cavity adjacent to the perforated plate or, alternately, with a resonant mode of the main duct of the flow system. Tsui and Flandro (1977) characterized a "singing" phenomenon associated with a main duct resonance and Ronneberger (1980) simulated such acoustic-coupled resonance using a single orifice. In addition to these types of shear layer instability-acoustic resonant coupling, which gives rise to pure tone oscillations, flow past perforated plates has been investigated from other perspectives, including the work of Nelson (1982), which is centered on broadband noise. More recent advances and overviews of this class of tonal instabilities are addressed by Howe (1998), Kirby and Cummings (1998), Dickey et al. (2001), and Jing et al. (2001).

Directly analogous to the foregoing oscillations of flow past perforated plates are the oscillations of flow past louvers, whereby the shear layer instability scales on the gap, or slot distance, between successive louvers, as described by Bruggeman et al. (1991) and Looijmans and Bruggeman (1997). In this case, the resonator is the cavity which bounds the louver system, and a depthwise acoustic mode is excited during the fully coupled state.

1.4. Self-excited, long wavelength oscillations of shear flow past a perforated/slotted plate

For all of the cases of resonant-coupled instabilities described in the foregoing, that is, instabilities of flow past a perforated plate, or a system of louvers, the inherent instability scales on the diameter of the perforation or the gap distance between louver plates; in turn, this instability couples with an acoustic resonant mode of the bounding cavity.

In recent years, a new type of purely hydrodynamic, long wavelength instability along perforated and slotted plates has been defined. It can occur in absence of acoustic or gravity wave resonant effects. Celik and Rockwell (2002, 2004), Ozalp et al. (2003), and Sever and Rockwell (2005) defined various aspects of this type of hydrodynamic instability. Ekmekci and Rockwell (2003) preliminarily reported on its coupling with a resonant mode of the bounding cavity. In parallel with these efforts, Zoccola (2002, 2004) characterized certain features of coupling between this instability and a resonant mode of the bounding cavity, and, in addition, Zoccola (2004) evaluated, for the first time, an energy integral for these oscillations due to flow past a slotted plate.

Generally speaking, the underlying physics of the resonant coupling between the inherent hydrodynamic instability past a perforated (or slotted) plate and a bounding resonant cavity has received very little attention, irrespective of whether the resonance involves an acoustic or gravity standing wave.

1.5. Unresolved issues

Taking into consideration the range of investigations described in the foregoing, it is possible to define unresolved issues, which provide a basis for the present investigation.

(i) Self-excited oscillations of flow past a cavity, whereby the separated shear layer along the cavity couples with a resonant mode of the cavity, have been investigated extensively for several configurations, primarily for flows of large spanwise extent, rather than for shallow flows. Generally speaking, experimental, wholefield characterization of the instantaneous and averaged structure of the cavity shear layer has not been addressed for the sequence of states that leads to a fully coupled oscillation. That is, the structure of the shear layer-cavity system is expected to be a strong function of the degree of lock-on of the shear layer to the resonant mode of the cavity. The sequence of states from a non-locked-on to a fully locked-on condition, which can be achieved by increasing the flow velocity, have not been determined via quantitative visualization.

(ii) For the case of shear flow along a perforated or slotted plate, placed along the mouth of the cavity, the flow structure is fundamentally different from the fully separated free-shear flow. The issue arises as to how self-excited oscillations of this shear flow couple with a longitudinal resonant mode of the cavity. The structure of the unsteady, resonant-coupled shear layer past a slotted plate, relative to the structure of the corresponding free-shear layer, i.e., in absence of the slotted plate along the cavity, has not been related to the sequence of states from a non-locked-on to a locked-on oscillation. More specifically, the structure of the flow patterns within the gaps of the plate, in relation to the flow patterns on either side of the plate, has remained unexplored for both the partially and fully coupled system. Furthermore, the degree to which the fully coupled, locked-on patterns are dependent upon the open area ratio of the plate has not been addressed.

(iii) Irrespective of whether one considers oscillations of a free-shear layer along the cavity opening, or oscillations along a slotted plate placed at the cavity opening, global, quantitative imaging can provide both instantaneous and time-averaged patterns of the flow states of highly coupled oscillations of the shear layer with the resonant mode of the adjacent cavity, as well as the states leading up to the fully coupled condition. That is, the nature of such global patterns has not been addressed for the case where the flow structure undergoes transformation from a purely hydrodynamic oscillation to an oscillation coupled with a resonant mode. More specifically, global, instantaneous representations of patterns of vorticity, Reynolds stress correlation and velocity fluctuations, can be interpreted in conjunction with their time-averaged counterparts. Furthermore, such global images can be acquired in a cinema sequence, thereby allowing evaluation of autospectra and cross-spectra over the entire domain of interest, based on the same time record. As a result, time-averaged phase patterns of a characteristic velocity fluctuation can provide still additional insight into the transformation from purely hydrodynamic oscillations to oscillations strongly coupled with a resonant mode. To date, these approaches have not been employed for the wide variety of self-sustaining, resonant, coupled oscillations occurring in different configurations.

The overall aim of this investigation is to address these unresolved issues. A technique of high-image-density particle image velocimetry is employed in conjunction with a free-surface water facility, which allows simulation of coupled

resonant phenomena that occur in gas systems, but at substantially reduced speeds and frequencies, thereby allowing adequate temporal resolution of a sequence of instantaneous images. Post-processing of the quantitative flow patterns allows a direct comparison between cavity oscillations without and with a slotted plate, thereby provide insight into the coupling mechanisms for these two classes of configurations.

2. Experimental system and techniques

Experiments were performed in a large-scale water channel. The main test-section of this channel has a depth of 610 mm, a width of 610 mm, and a length of 5484 mm. A major objective of the present series of experiments was to determine the structure of: a free-shear layer along the cavity opening; and a shear layer along a slotted plate along the cavity opening. Of particular interest are the states of non-coupled, marginally coupled, and fully coupled shear-layer oscillations with the free-surface (gravity wave) resonant mode of the cavity. To achieve these objectives, it was necessary to design and construct a test-section insert, which allowed control of the water depth and the inflow to the resonant cavity-slotted plate system.

Fig. 1 shows a portion of a horizontal long (plexiglas) plate which supported the cavity-vertical plate system. This plate of thickness 12.7 mm was located at an elevation of 232 mm above the floor of the main test-section and extended a distance of 1042 mm downstream of the leading-edge of the cavity. The vertical plate that connects to the cavity, as shown in Fig. 1, extended from a contraction having an inlet width of 610 mm and an outlet width of 152.4 mm. The shallow water layer flowed through this constant cross-section of 152.4 mm for a distance of 1790 mm upstream of the cavity. With this arrangement, it was possible to attain a fully turbulent boundary layer at the leading-corner of the cavity.

A zoomed-in representation of the dimensions of the slotted plate system is given in Fig. 2, which designates the thickness w of each slat, the gap G between the slats, and the width t of the slats. A range of values of these parameters was employed during preliminary experiments, in order to determine the configurations that yielded the most pronounced, self-excited oscillations. Then, variations on these parameters were considered in order to demonstrate detuning of the oscillations.

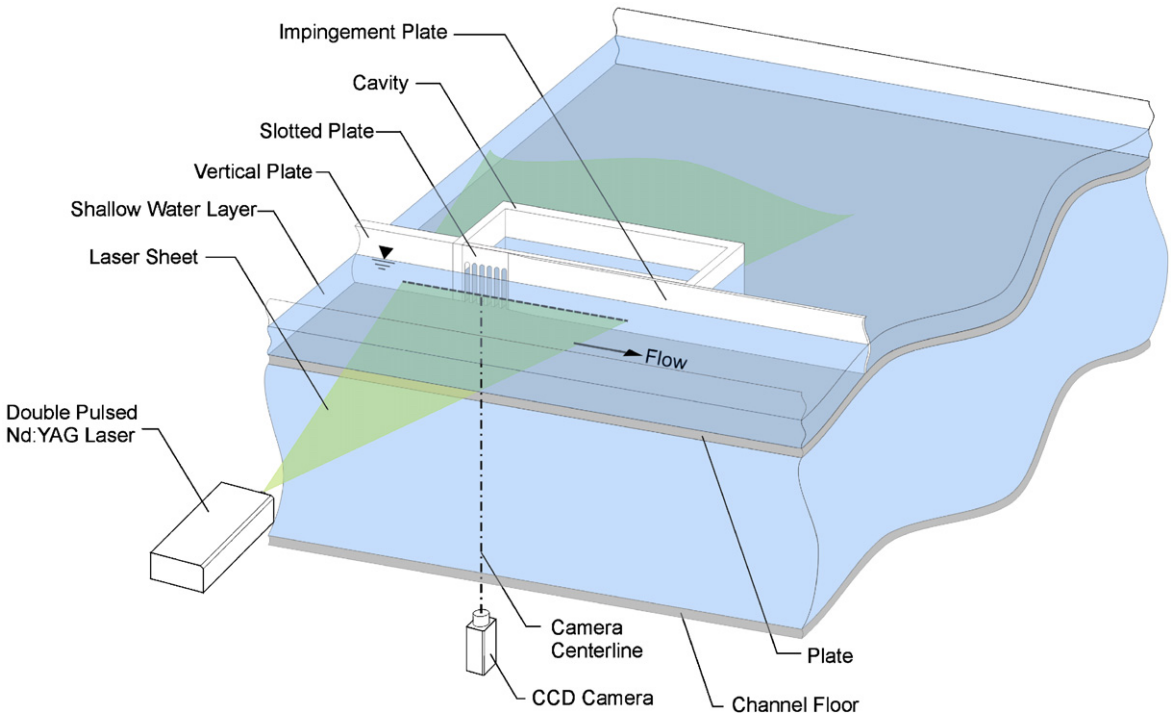

Fig. 1. Experimental facility.

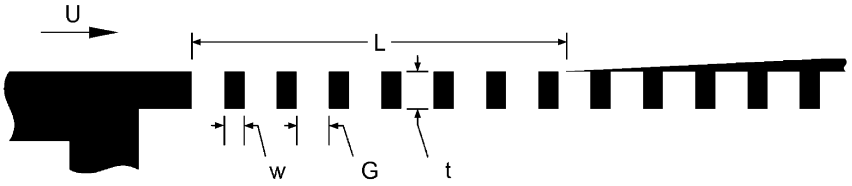

Fig. 2. Definition of parameters of slotted plate system.

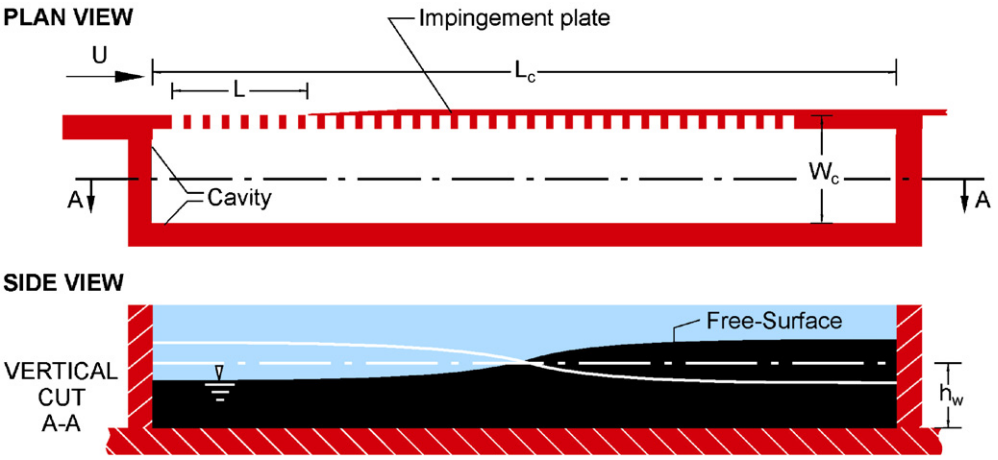

Fig. 3. Schematic of slotted plate-resonant cavity system showing first mode of free-surface resonance at section A–A. For purposes of illustration, vertical deflection of free-surface is magnified.

Furthermore, Fig. 3 gives an overview of the slotted plate-cavity system. The schematic of the first longitudinal resonant mode of the gravity wave is depicted in the sectional side view of Fig. 3. Referring to the dimensions in the plan view of Fig. 3, the cavity section has an internal length $L_c = 304.8$ mm and an internal width $W_c = 76.2$ mm. The vertical, slotted plate was placed flush with the leading-corner of the cavity. The vertical plexiglas impingement plate with a streamwise length of 762 mm could be adjusted to various positions in the streamwise direction, in order to vary the effective length L of the slotted plate or, when the slotted plate was removed, the effective length L of the cavity. During the course of experiments, this length was varied from $L = 53.2$ to 63.5 mm.

By adjusting the level of water in the test-section, it was possible to attain an arbitrary value of h_w, designated in Fig. 3. A value of $h_w = 38.1$ mm, which was associated with the largest amplitude, resonant-coupled oscillations, was employed for the major share of experiments, involving detailed characterization of the free-shear flow and the shear flow along the slotted plate, including the range of states from non-locked-on to locked-on (fully coupled) cases (Sections 3–6). For experiments that characterized the effect of plate geometry on oscillations of shear flow past the slotted plate, in presence of the resonant cavity (Section 7), a value of $h_w = 25.4$ mm, which yielded well-defined, resonant-coupled oscillations, was employed in order to accommodate the different geometries of the slotted plates.

For the case of the free-shear layer past the cavity, i.e., no slotted plate along the mouth of the cavity, the values of Reynolds number based on the width W of the inflow channel and the momentum thickness θ of the boundary layer were respectively $\mathrm{Re}_W = 43\,554$ and $\mathrm{Re}_\theta = 746$ at a value of inflow velocity $U_r = 286.5$ mm/s, which corresponded to the fully coupled resonant state of the cavity oscillation. Since the patterns of flow structure associated with the onset of a resonant state are important, the inflow velocity was varied from a minimum value of $U = 172.8$ mm/s to the aforementioned maximum of $U_r = 286.5$ mm/s. The states of the flow corresponding to $U/U_r = 0.60$, 0.81 and 1.00 were examined in detail.

For oscillations of the shear layer along the slotted plate, a plate with dimensions $w^* = w/\theta = 1.71$ and $G^* = G/\theta = 2.86$ was employed, in which θ is the inflow momentum thickness at the resonant condition. This configuration yielded highly coherent oscillations. The Reynolds numbers, which were close to the foregoing values for the free-shear layer along the cavity, were respectively $\mathrm{Re}_W = 47\,942$ and $\mathrm{Re}_\theta = 701$ at a value of inflow velocity $U = 315.4$ mm/s, which corresponded to the velocity U_r of the fully coupled resonant state of the cavity oscillation. The inflow velocity

was varied from a minimum value of $U = 177\,\text{mm/s}$ to the maximum value of $U_r = 315.4\,\text{mm/s}$. Detailed characterization of flow structure was performed for values of $U/U_r = 0.56$, 0.74 and 1.00.

The frequency of the first longitudinal mode of gravity wave resonance of the cavity was excited; it had the same value of $f_r = 1.44\,\text{Hz}$ for both the aforementioned cases of the free-shear and the shear layer along the slotted plate. The frequency response of the system as it approaches its resonant state is illustrated on the plot of shear layer oscillation frequency f_o normalized by f_r, i.e., f_o/f_r, versus U/U_r as given in Fig. 4. The data points therefore correspond to the progressive onset of resonance as U/U_r increases; at resonance, highly coherent, self-sustained oscillations occur, for cases without and with the slotted plate. It is evident that the variation of f_o/f_r for both of these two basic types of systems is remarkably similar. At $U/U_r = 1.0$, the values of inverse Strouhal number are $U/f_rL = 3.12$ and 4.16, respectively, for the free-shear layer and the shear layer along the slotted plate.

Experiments were also performed to determine the effect of plate geometry on the degree of coupling between oscillations of the shear layer past the slotted plate placed at the mouth of the cavity with the longitudinal resonant mode of the gravity wave. The flow structure was characterized for plate geometries of: $w^* = w/\theta = 0.5$, $G^* = G/\theta = 2.5$; $w^* = 1.0$, $G^* = 2.5$; $w^* = 1.5$, $G^* = 2.5$; and $w^* = 1.0$, $G^* = 5.0$. For all cases, the plate thickness was maintained at $t^* = t/\theta = 2.2$. During these experiments, the values of Reynolds number based on the width W of the inflow channel and the momentum thickness θ of the boundary layer were respectively $\text{Re}_W = 36\,864$ and $\text{Re}_\theta = 630$ at a value of inflow velocity $U_r = 242.5\,\text{mm/s}$ for which resonance occurred.

Quantitative imaging of the instantaneous flow patterns of the unsteady flow past and within the cavity, both without and with the slotted plate, was accomplished using a digital version of particle image velocimetry (DPIV). The flow was seeded with 14 μm, metallic-coated particles. Illumination was provided by a double-pulsed Nd:Yag laser system. The collinear beams were transmitted through a combination of spherical and cylindrical lenses, in order to produce a laser sheet of thickness of approximately 1 mm. As illustrated in Fig. 1, this laser sheet was positioned in a horizontal plane, at an elevation of 12.7 mm above the bottom surface of the cavity test-section. In order to allow optimal evaluation of the particle image patterns to yield velocity vectors, the time delay between pulses of the double-pulsed laser system was from 1.0 to 1.5 ms, depending upon the inflow velocity U. For acquisition of images, a digital charge-coupled device (CCD) camera was used to record the patterns of particle images. This camera had a total of 1024 horizontal and 1024 vertical pixels, of which 1008 and 1018 pixels in the horizontal and vertical directions respectively are light sensitive. The active imager area has a size of $9.0\,\mu\text{m} \times 9.0\,\mu\text{m}$. The camera was equipped with a lens of total length 60 mm, thereby providing a magnification of 1:8.3. The aforementioned double-pulsed laser and camera were triggered by a synchronizer. The camera operated at thirty frames/s, which gives fifteen sets of image pairs per second.

Processing of the particle image patterns involved a cross-correlation technique. Interrogation windows of 32×32 was employed, with an effective overlap of 50% in order to satisfy the Nyquist criterion. This approach yielded a total of 23×53 velocity vectors. Post-processing of the raw velocity field involved automatic validation of the vector field by removal of spurious spectra, replacement of these spurious vectors using a bilinear interpolation technique, and implementation of a Gaussian filter with an exponent of $p = 1.3$. The total number of spurious vectors, however, was less than 2% of the total number of vectors.

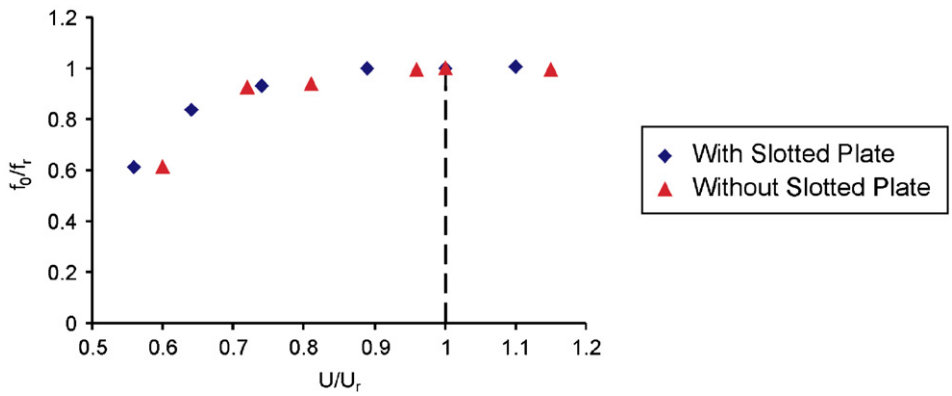

Fig. 4. Oscillation frequency f_o, normalized by resonant frequency f_r of cavity, versus inflow velocity U, normalized by its value U_r at resonance.

3. Overview of oscillations without and with slotted plate

A central goal of the present investigation is to characterize the detailed flow structure arising from coupling between the unsteady shear layer along the mouth of the cavity and the resonant oscillations of the free-surface within the cavity. This characterization involves, first of all, the shear layer in absence of a slotted plate, then in presence of the plate. This approach allows detailed quantitative insight into each of these basic cases and, furthermore, allows a direct comparison between them. The aim is, first of all, to gain an understanding of the detailed flow structure during resonant coupling of a free-shear layer, and, second, to define the distinctive features of the resonant-coupled unsteady shear flow past the slotted plate system.

In describing details of each of the basic cases of oscillation, i.e., without and with the slotted plate along the mouth of the cavity, it is helpful to directly compare selected, key features of the instantaneous structure, as given in Fig. 5. These instantaneous images were selected using a phase-referencing criterion, which corresponds to the appearance of a large-scale vorticity concentration at a location immediately upstream of the tip of the edge, as indicated by the vorticity patterns at $t/T = 1.0$ in the images without and with the slotted plate; t is the time and T is the period of the oscillation. Then, earlier phases of the oscillation cycle are represented for smaller values of $t/T = 0.4$ and 0.7; these same values of effective phase during the oscillation cycle, i.e. same t/T, are employed for shear flows in absence and in presence of a slotted plate. The relation of the aforementioned criterion for defining the reference time $t/T = 1.0$ could not be related to the phase of the unsteady deflection of the free-surface with the present experimental technique.

Comparison of the patterns of vorticity at successively larger values of t/T shows, for the case of the free-shear flow in the top set of images of Fig. 5, development of a well-defined, large scale cluster of negative vorticity, which culminates in the large-scale cluster at $t/T = 1.0$; moreover, at this instant, the instantaneous shear layer, represented by the train of small-scale vorticity concentrations between the large-scale cluster of vorticity and the leading-corner of the cavity, is deflected substantially from its equilibrium position along the mouth of the cavity.

For the case of unsteady shear flow past the slotted plate, shown in the bottom set of images of Fig. 5, at $t/T = 0.4$, small-scale vorticity concentrations form between the slats of the slotted plate. Not until $t/T = 0.7$ does an identifiable, larger-scale cluster of vorticity appear above the slotted plate. At a later time $t/T = 1.0$, the spatial extent of this larger-scale cluster of vorticity increases in size as it convects along the upper surface of the plate, as shown in the vorticity image at $t/T = 1.0$.

Corresponding patterns of instantaneous Reynolds stress correlation $u'v'/U^2$ are shown in the right columns of the sets of images of Fig. 5. These instantaneous products $u'v'/U^2$ were evaluated from the same set of velocity data as for the aforementioned patterns of vorticity. For the free-shear flow past the cavity, the sequence of images of $u'v'/U^2$ at successively larger values of t/T shows the development of increasingly larger-scale, higher amplitude patterns of negative $u'v'/U^2$. For the flow past the slotted plate, patterns of negative $u'v'/U^2$, of substantially smaller spatial extent and peak values, are identifiable at all values of t/T. At the smallest value of $t/T = 0.4$, the pattern of $u'v'/U^2$ located at the upper right of the image, i.e., above the surface of the impingement plate, is apparently due to the previous cycle of oscillation. The small, elongated pattern located above the plate is apparently due to coherent fluctuations of the pattern of small-scale structures along its upper edge. At the next instant of the sequence, shown at $t/T = 0.7$, the larger-scale pattern of negative $u'v'/U^2$ occurs near the leading region of the plate, and is apparently associated with the onset of the larger-scale instability. Further development of this pattern is shown at $t/T = 1.0$; at this instant, the region of $u'v'/U^2$ has moved further downstream along the upper surfaces of the plate, and has a larger spatial extent and peak value.

From this brief overview of Fig. 5, it is evident that a shear flow past a slotted plate located along the mouth of a resonant cavity system can lead to organized oscillations, presumably due to coupling between the shear layer and a resonant free-surface mode within the cavity. The mechanism of hydrodynamic instability of this special class of the shear layer along the slotted plate shows features distinctly different from the corresponding free-shear layer instability. From a theoretical standpoint, the instability of the free shear flow along the cavity arises from a classical Kelvin–Helmholtz (K–H) instability. On the other hand, the instability along the slotted plate configuration cannot arise from a K–H instability, since the steady (time-mean) distribution of velocity across the shear flow is fundamentally different. In fact, this latter type of instability involves a complex interaction between unsteady, small-scale clusters of vorticity within the slots of the plate, onset and development of a large-scale cluster of vorticity, and an alternating jet flow at the trailing-edge of the slotted plate.

In the following sections, cases of the free-shear layer and the shear layer along the slotted plate are characterized in detail, and the corresponding images are presented in such a fashion as to allow direct comparison between these two basic cases.

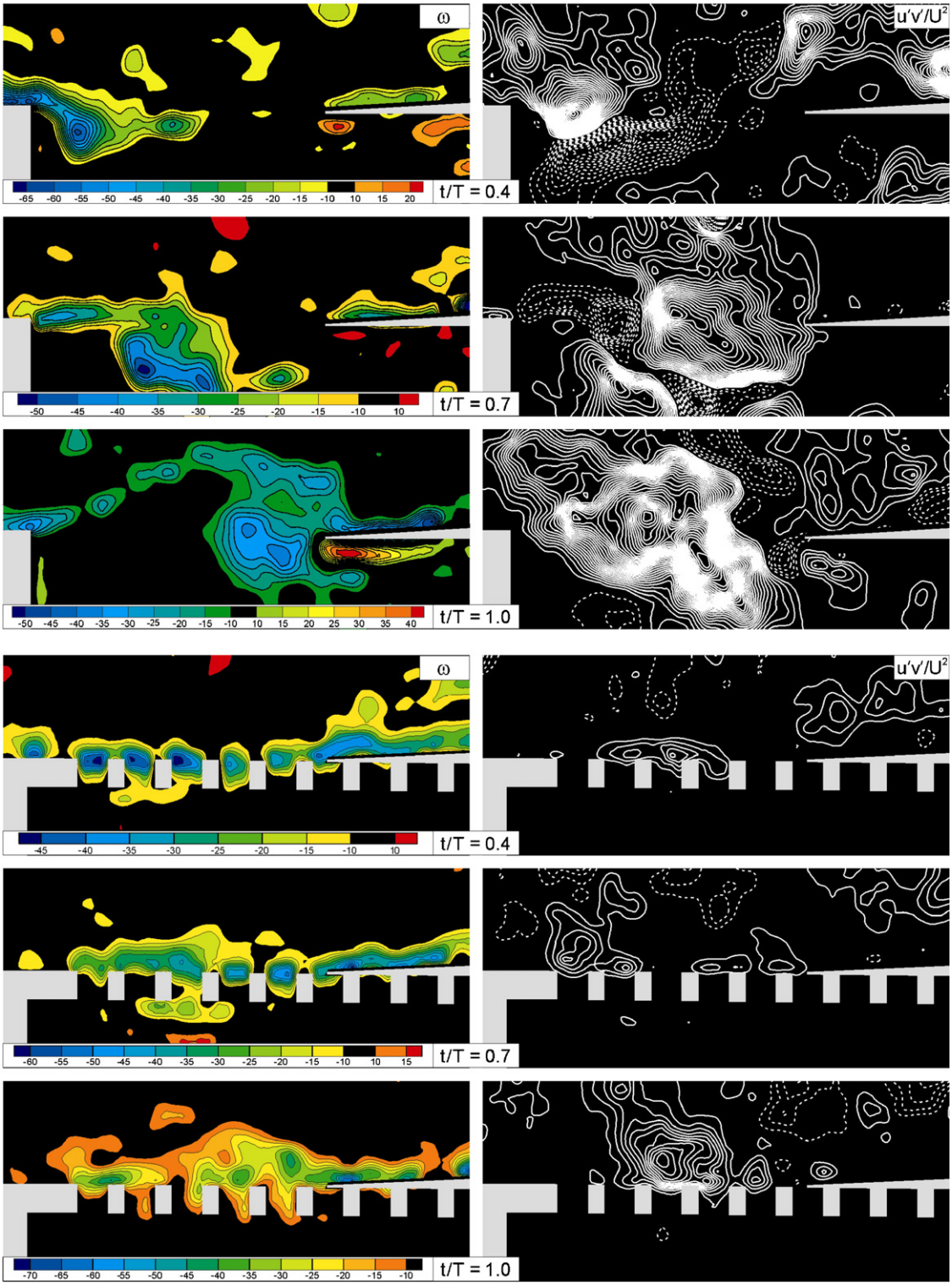

Fig. 5. Comparison of patterns of instantaneous vorticity ω and velocity correlation $u'v'/U^2$ for cases without and with a slotted plate. Minimum and incremental values of vorticity are $|\omega|_{\min} = 10\,s^{-1}$ and $|\Delta\omega| = 5\,s^{-1}$. Minimum and incremental values of velocity correlation are $|[u'v'/U^2]|_{\min} = 0.005$ and $|\Delta[u'v'/U^2]| = 0.005$. For the contours of constant velocity correlation, solid lines are negative and dashed lines are positive values. Images for the slotted plate at $t/T = 0.7$ and 1.0 are from Ekmekci and Rockwell (2003).

4. Oscillations of a free-shear layer past a resonant cavity

4.1. Time-averaged flow structure

The case of the free-shear layer past the cavity opening is represented in Fig. 6. Three sets of patterns are illustrated; they correspond to values of the free-stream velocity U, normalized with respect to the value of free-stream velocity U_r at which locked-on resonance occurs. The values of $U/U_r = 0.60$, 0.81 and 1.00 can be interpreted with the aid of Fig. 4, which shows the approach of the frequency ratio f_o/f_r to a value of 1.0 as U/U_r approaches 1.0. At each value of U/U_r, patterns of averaged velocity vectors $\langle V\rangle/U$, streamwise distributions of velocity $\langle u\rangle/U$, streamlines $\langle\psi\rangle$ and vorticity $\langle\omega\rangle$ are given. Comparison of the patterns of averaged velocity $\langle V\rangle/U$ and streamlines $\langle\psi\rangle$ shows that as the value of U/U_r increases, a large-scale (clockwise) recirculation cell sets in. The other half of the cell is evident in the lower part of the image of streamlines $\langle\psi\rangle$ at $U/U_r = 1.00$. Concerning the distributions of streamwise velocity $\langle u\rangle/U$, an inflection point is evident in the distribution for all values of U/U_r. As U/U_r increases, however, the location of this inflection point shifts downward into the cavity. In turn, this downward shift is associated with downward deflections of the pattern of vorticity $\langle\omega\rangle$ for increasing values of U/U_r. This type of distortion of the pattern of average vorticity $\langle\omega\rangle$ is associated with the very large oscillation amplitudes of the shear layer past the cavity at large values of U/U_r. All patterns of vorticity $\langle\omega\rangle$ show two extrema of vorticity. The first occurs at the leading corner of the cavity. It takes the form of a highly concentrated region at $U/U_r = 1.00$, apparently due to the interaction of the resonant free-surface wave field with the corner. The other region of relatively high vorticity occurs along the surface of the impingement edge; it has the form of a relatively elongated region of higher-level vorticity, which is associated with the interaction between the undulating shear layer and the edge.

4.2. Instantaneous flow structure

The averaged patterns described in the foregoing are a consequence of the sequence of instantaneous states of the flow in Fig. 7. Distributions of instantaneous velocity vectors V/U, fluctuating velocity vectors V'/U, vorticity ω and Reynolds stress correlation $u'v'/U^2$ are shown for the same three values of velocity ratio $U/U_r = 0.60$, 0.81 and 1.00, as addressed in Fig. 6. These instantaneous patterns were selected according to the following phase criterion: occurrence of a large-scale cluster of negative vorticity at a location immediately upstream of the tip of the edge. This criterion is evident from comparison of the patterns of vorticity ω at the three different values of U/U_r.

Considering, first of all, the patterns of instantaneous velocity V/U, flow is ejected vertically from the cavity region into the free-stream at all values of U/U_r. The magnitude and extent of this ejected flow is, however, increasingly pronounced with larger values of U/U_r. That is, at the limiting value of $U/U_r = 1.00$, the ejected fluid substantially penetrates into the region above the elevation of the sharp edge, in contrast to the pattern at the lower value $U/U_r = 0.60$.

Corresponding patterns of instantaneous velocity fluctuation V'/U in Fig. 7 also show this ejection. It is evident that the vectors V'/U of the ejected flow tend toward a vertical orientation at the highest value of $U/U_r = 1.00$, relative to their highly inclined orientations at the smallest value of $U/U_r = 0.60$. In addition, these patterns of V'/U clearly show a well-defined swirl region located immediately upstream of the tip of the impingement edge. In fact, these swirl patterns are in accord with the appearance of the large-scale concentration of vorticity ω at that location.

In the patterns of vorticity ω of Fig. 7, the angle of inclination of the separating shear layer from the leading-corner of the cavity increases with increasing values of U/U_r. That is, it is deflected at only a small angle, i.e., it is nominally horizontal at $U/U_r = 0.60$ and increases to an angle of approximately 30° at $U/U_r = 1.00$.

All of the foregoing processes are associated with increasing magnitude and spatial extent of the normalized, instantaneous velocity correlation $u'v'/U^2$ along the region between the leading-corner of the cavity and the leading-edge of the impingement edge. The peak values of $u'v'/U^2 = -0.047$, -0.080 and -0.185 respectively for $U/U_r = 0.60$, 0.81 and 1.00. It is therefore evident that the large-amplitude deflections of the shear layer and formation of a prevalent cluster of vorticity ω at the resonance condition $U/U_r = 1.00$ are associated with highly correlated velocity fluctuations $u'v'/U^2$. That is, clusters of $u'v'$ are an indication of the strength and degree of coherence of the organized structure in the separated shear layer. They complement the patterns of instantaneous vorticity ω. Comparison of patterns of vorticity with patterns of instantaneous Reynolds stress correlation in Fig. 7 shows, for successively larger values of U/U_r, that when the peak value of ω increases, the peak magnitude of $u'v'/U^2$ increases as well.

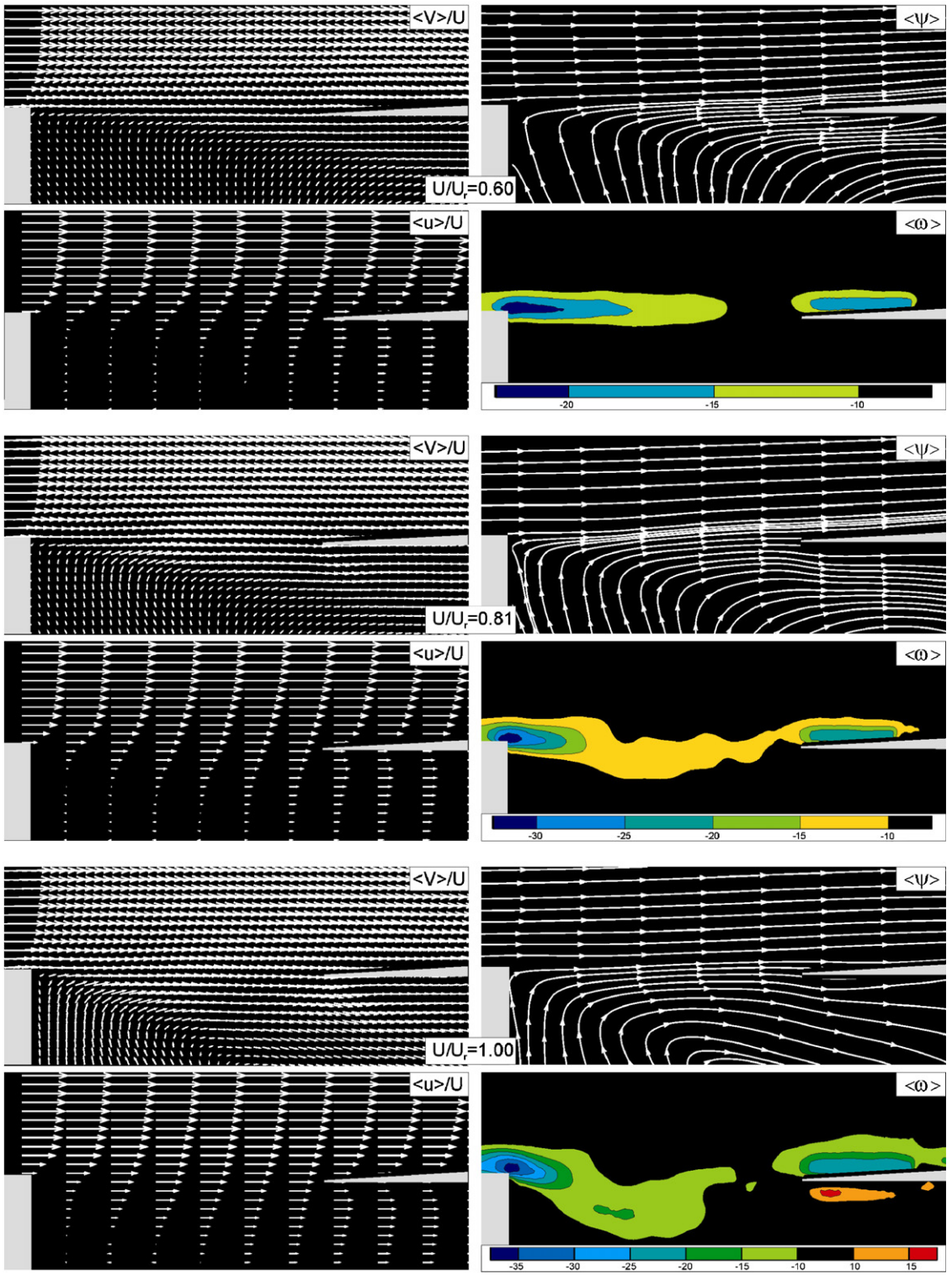

Fig. 6. Comparison of time-averaged patterns of velocity $\langle V \rangle / U$, streamwise component of velocity $\langle u \rangle / U$, streamlines $\langle \Psi \rangle$ and vorticity $\langle \omega \rangle$. Images are shown for three different values of velocity ratio U/U_r, which represents the ratio of the free-stream velocity U to its value at the resonance condition. For the patterns of vorticity, the minimum and incremental values are $|\omega|_{\min} = 10$ and $|\Delta\omega| = 5\,\mathrm{s}^{-1}$. The zeroth level and the first levels above and below zero are omitted for the clearer illustration of the flow structure.

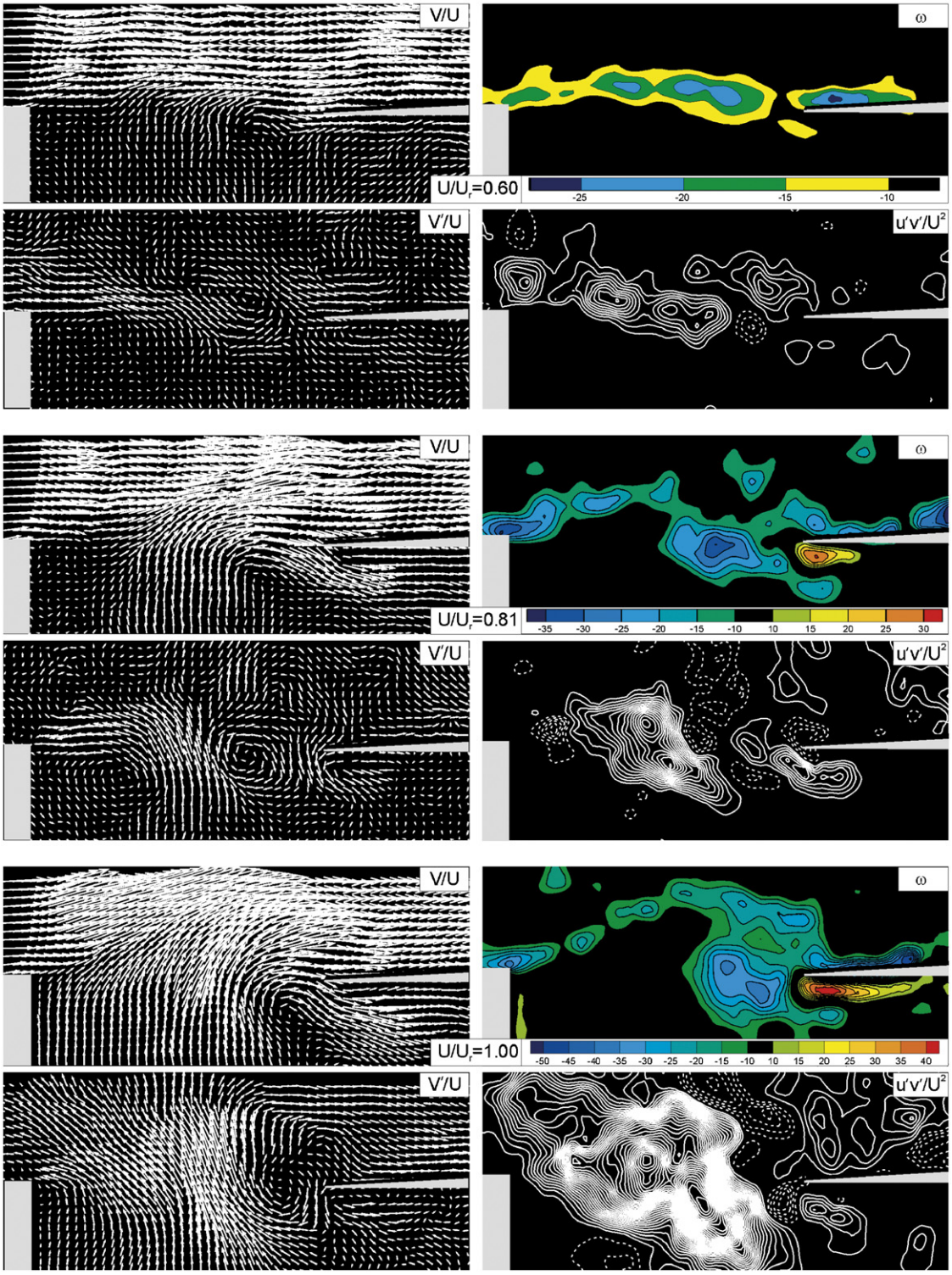

Fig. 7. Patterns of instantaneous velocity V/U, velocity fluctuation V'/U, vorticity ω and velocity correlation $u'v'/U^2$ for three values of the ratio of free-stream velocity U to its value at U_r at the resonance condition. For patterns of vorticity, the minimum and incremental values are $|\omega|_{\min} = 10$ and $|\Delta\omega| = 5\,\mathrm{s}^{-1}$. For the contours of constant velocity correlation, the minimum and incremental values are $|[u'v'/U^2]|_{\min} = 0.005$ and $|\Delta[u'v'/U^2]| = 0.005$; solid lines are negative and dashed lines are positive values.

4.3. Time traces and spectra

Fig. 8 shows representative time traces $u(t)$ and spectra $S_u(f)$ of the streamwise u component of the velocity fluctuation at the same values of velocity ratio $U/U_r = 0.60$, 0.81 and 1.00. These representations are indicated for three locations a, b and c at each value of U/U_r. The patterns shown in the images of Fig. 8 represent contours of constant magnitude of autospectral density $|S_u(f_o)|$. These contours were constructed by considering the peak amplitude at the most coherent frequency f_o of oscillation. It is evident from the pattern at $U/U_r = 0.60$ that the amplitude of the autospectral density at f_o is very small. For successively higher values of $U/U_r = 0.81$ and 1.00, the amplitudes increase substantially.

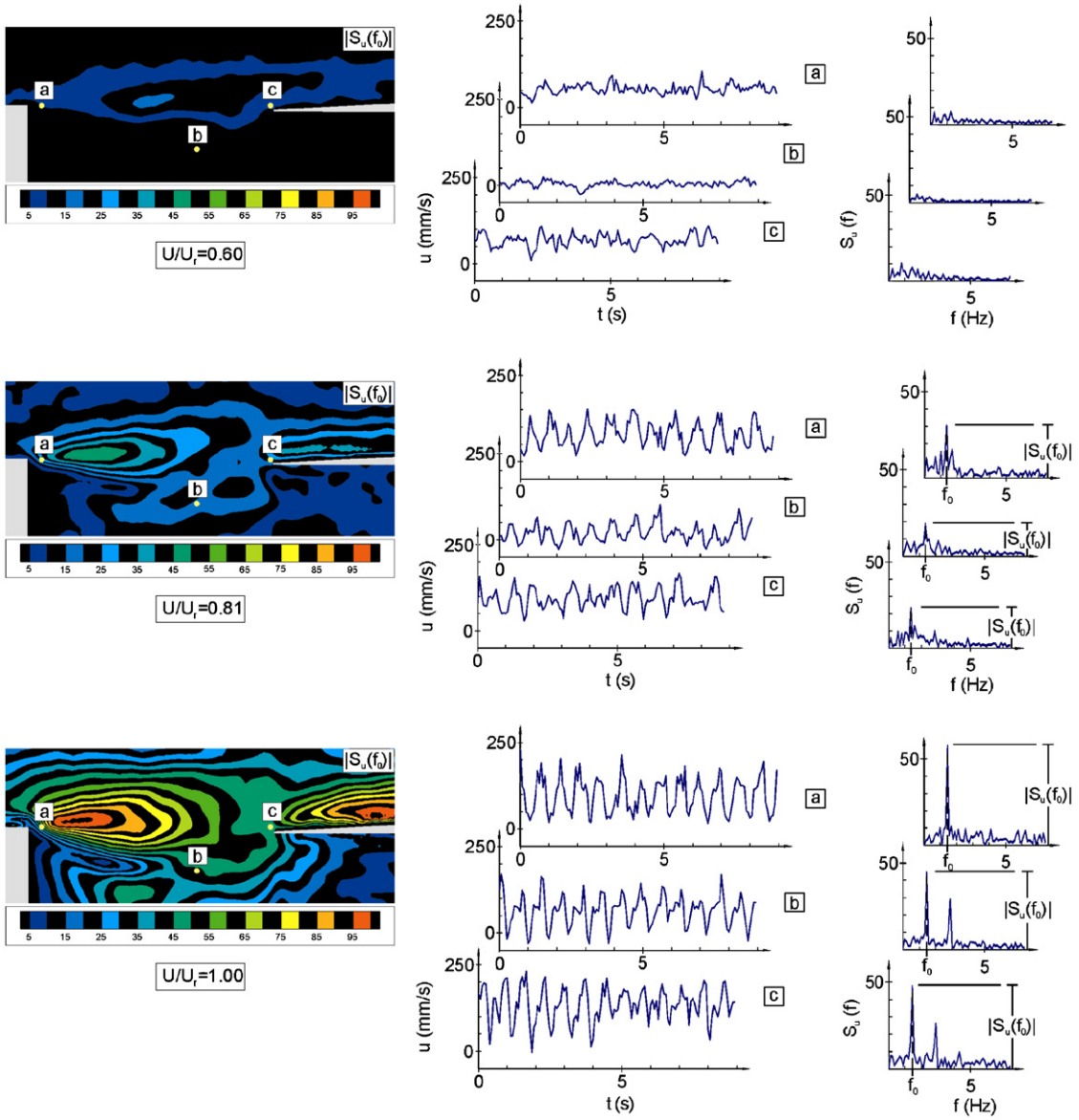

Fig. 8. Images showing contours of constant peak amplitude of autospectral density $|S_u(f_o)|$ of fluctuating streamwise velocity u at predominant frequency f_o, and representative values of time traces of streamwise velocity u and spectra $S_u(f)$. These images and plots are shown for three values of velocity ratio U/U_r, in which U is the free-steam velocity and U_r corresponds to its value at the resonance condition. Minimum and incremental values are $[|S_u(f_o)|]_{\min} = 5$ and $\Delta[|S_u(f_o)|] = 5$.

Time traces at the selected locations a, b and c show the transformation from ill-defined time traces to those having a quasi-periodic form, for increasing values of U/U_r. The corresponding spectra show, at the lowest value $U/U_r = 0.60$, no detectable peak, then emergence of a significant, and finally a pronounced peak at successively higher values of $U/U_r = 0.81$ and 1.00. In fact, at $U/U_r = 1.00$, the oscillation is of sufficiently high amplitude as to generate both a fundamental and a harmonic.

Furthermore, if one considers, at each value of U/U_r, the time traces and spectra at locations a, b and c, it is evident that they have the same general form. This observation indicates that the onset of the well-defined oscillation at higher values of U/U_r is a globally coupled phenomenon between the cavity shear layer and the resonant mode of the cavity. That is, if one considers, for example, the time traces and spectra at $U/U_r = 0.81$ and $U/U_r = 1.00$, the peak amplitude does not appear to increase exponentially with streamwise distance from the leading-corner of the cavity, as it would for the case of a linearly amplifying disturbance in absence of coupling with the resonant mode of the cavity (Knisely and Rockwell, 1982). Apparently, the occurrence of resonance induces large-amplitude fluctuations of velocity and vorticity in the vicinity of the leading-corner of the cavity, which then persists in the streamwise direction.

4.4. Time-averaged representations of the fluctuating flow structure

Fig. 9 shows averaged representations of the unsteady flow field. These patterns include the root-mean-square of the transverse (vertical) velocity fluctuation v_{rms}, and the corresponding root-mean-square of the streamwise (longitudinal) velocity fluctuation u_{rms}, both normalized with respect to the free-stream velocity U of the incident flow. Furthermore, patterns of averaged Reynolds stress correlation $\langle u'v' \rangle / U^2$ and phase angle $\Phi_u(f_o)$ at the predominant frequency f_o are also illustrated.

Consider, first of all, the contours of constant v_{rms}/U at $U/U_r = 0.60$. The levels are relatively low, the center of the pattern is located close to the tip of the impingement edge, and the peak value of v_{rms}/U is only 0.086. At higher values of $U/U_r = 0.81$ and 1.00, the peak level increases substantially to values, respectively, of 0.253 and 0.342. At $U/U_r = 1.00$, the peak has moved to a location further upstream and, furthermore, is displaced below the line connecting the leading-corner of the cavity and the tip of the impingement edge. Regarding the movement of the maximum (peak) value of v_{rms} into the cavity, it is most likely due to a change in the pattern of the steady (time-mean flow) involving a balance between the entrained flow into the separated shear layer and the return flow into the cavity at the location of impingement, which is altered with increasing U/U_r. The large-amplitudes of transverse fluctuation are, of course, directly related to the patterns of ejected fluid shown in the instantaneous distributions of total velocity V/U and fluctuating total velocity V'/U in Fig. 7. (As suggested by a referee, it would be insightful, in further experiments of this type, to employ a phase-averaging process to the cinema sequence of images, with an appropriate phase reference, in order to determine the time-dependent volume flux through the mouth of the cavity as a function of time.)

Concerning the patterns of longitudinal velocity fluctuation u_{rms}/U, again at $U/U_r = 0.60$, the peak value has a magnitude of 0.157 and, for larger values of $U/U_r = 0.81$ and 1.00, the peak value rises respectively to 0.228 and 0.270 and, simultaneously, moves to a location close to the leading-corner of the cavity. This process is accompanied by increasingly larger values of u_{rms}/U in the region immediately above the surface of the impingement edge. These peak values are, respectively, $u_{\mathrm{rms}}/U = 0.141$, 0.188 and 0.297 for $U/U_r = 0.60$, 0.81 and 1.00. In other words, the aforementioned, substantial increase in root-mean-square velocity fluctuation amplitude described in the foregoing for the region along the cavity opening is accompanied by corresponding patterns of longitudinal fluctuation u_{rms}/U adjacent to the surface of the edge. This relationship indicates the increased global coupling between the undulating shear layer and the resonant mode of the cavity. The upstream movement of the maximum (peak) value of u_{rms} is due to the increased oscillation amplitude of the shear layer, which occurs with increasing U/U_r; it is directly analogous to upstream movement of the onset of nonlinearity of a separated shear layer as the amplitude of external excitation by a loudspeaker is increased.

Patterns of averaged Reynolds stress $\langle u'v' \rangle / U^2$ provide a further indicator of the increased coupling and thereby the amplitude of oscillation. Both the peak magnitude and spatial extent of these contours increases dramatically with the degree of coupling. Peak values of $\langle u'v' \rangle / U^2 = -0.008$, -0.025 and -0.045 are determined, respectively, for values of $U/U_r = 0.60$, 0.81 and 1.00. From a physical standpoint, the patterns of Reynolds stress correlation $\langle u'v' \rangle / U^2$ are an indication of the magnitude of the flow entrained into the separating shear layer as it evolves between the separation and impingement edge. In turn, this entrained flow is balanced by the returned flow into the cavity at the location of impingement, thereby resulting in changes in the flow physics in the immediate vicinity of the impingement edge. In fact, examination of Fig. 6 shows that, as the magnitude of U/U_r increases, the separated shear layer is deflected further into the cavity, in accord with the increasing level of Reynolds stress correlation, $\langle u'v' \rangle$, indicated in Fig. 7.

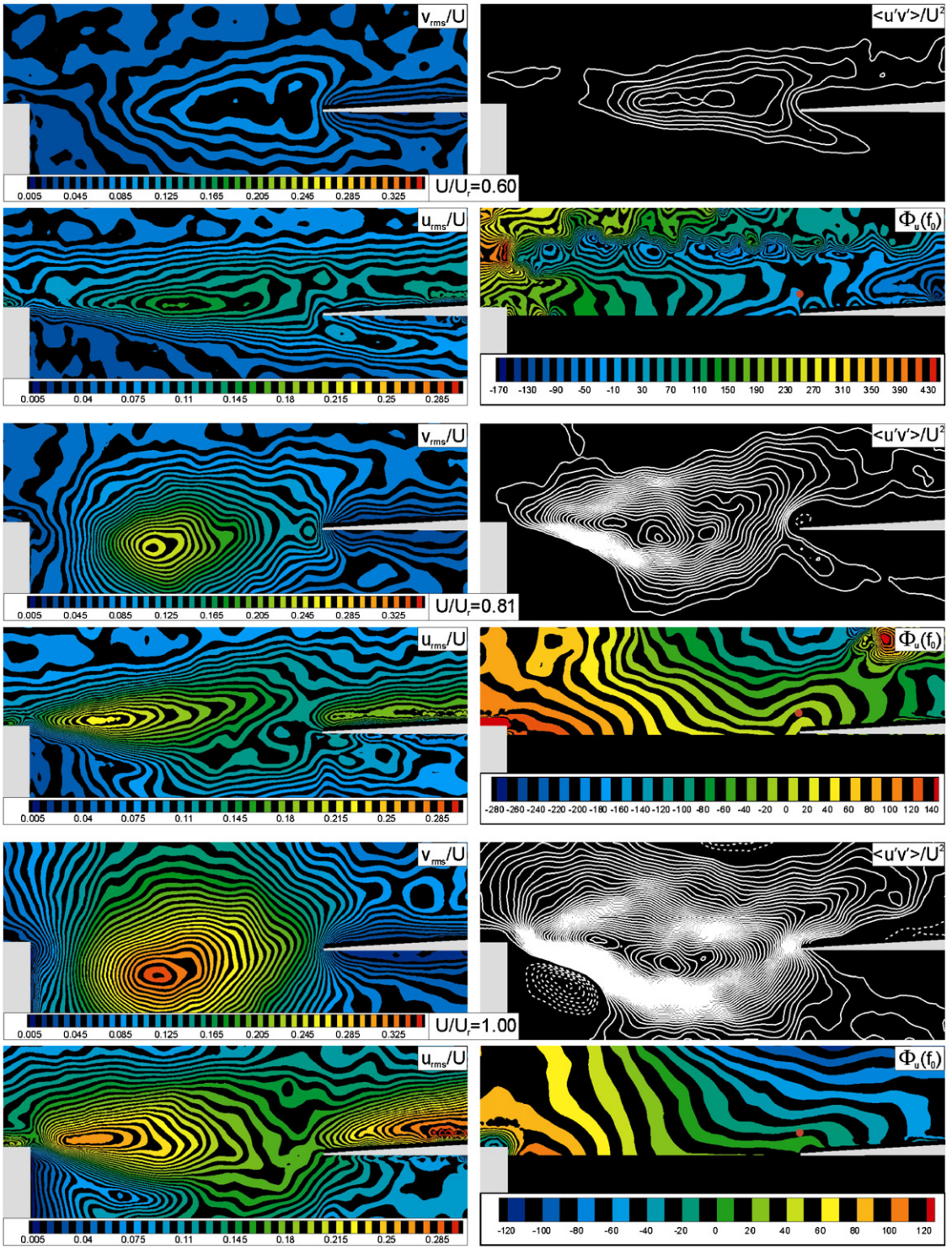

Fig. 9. Contours of constant transverse velocity fluctuation v_{rms}/U, longitudinal velocity fluctuation u_{rms}/U, Reynolds stress correlation $\langle u'v' \rangle / U^2$ and phase angle $\Phi_u(f_o)$ at predominant frequency, f_o, for three different values of U/U_r, in which U is the free-stream velocity and U_r is its value at the resonance condition. Minimum and incremental values of v_{rms}/U are $[v_{\mathrm{rms}}/U]_{\min} = 0.005$ and $\Delta[v_{\mathrm{rms}}/U] = 0.005$. For longitudinal velocity fluctuation u_{rms}/U, minimum and incremental values are $[u_{\mathrm{rms}}/U]_{\min} = 0.005$ and $\Delta[u_{\mathrm{rms}}/U] = 0.005$. For velocity correlation, $\langle u'v' \rangle / U^2$, minimum and incremental values are $|[\langle u'v' \rangle / U^2]|_{\min} = 0.002$ and $|\Delta[\langle u'v' \rangle / U^2]| = 0.001$; solid lines are negative and dashed lines are positive values.

A still further indicator of the degree of resonant coupling is provided by the contours of constant phase angle $\Phi_u(f_o)$, which were determined from the cross-spectrum of the streamwise velocity fluctuations at the predominant frequency f_o, at each grid point over the entire domain; the reference grid point was located at defined elevation from the tip of the impingement edge, designated by a dot in each image. These patterns are ill-defined at $U/U_r = 0.60$, due to substantial jitter of the low amplitude oscillation. Immediately prior to the onset of resonance ($U/U_r = 0.81$) and at resonance ($U/U_r = 1.00$), the phase contours exhibit a highly ordered form.

5. Oscillations of a shear layer along a slotted plate in presence of a resonant cavity

5.1. Time-averaged flow structure

Fig. 10 shows the time-averaged patterns corresponding to an unstable shear flow past a slotted plate located at the mouth of the cavity, for three successive values of U/U_r, in which, as in the preceding terminology, U is the inflow free-stream velocity and U_r is its value at the resonant oscillation condition $f_o/f_r = 1.0$. These parameters are represented in Fig. 4. For all values of U/U_r, the layer along the upper surface of each slat takes the form of a bounded shear flow, i.e., no point of inflection exists in the distribution of $\langle u \rangle/U$. On the other hand, below the slotted plate, a counterflow occurs, that is, the direction of the arrows representing $\langle u \rangle/U$ is in a direction opposite to those above the plate. Further aspects of this counterflow are evident in the patterns of time-averaged streamlines $\langle \Psi \rangle$. This region of counterflow beneath the slotted plate appears to be part of a large-scale recirculation cell and, by comparison of the images at $U/U_r = 0.56$, 0.74 and 1.00, it appears that the center of this recirculation cell moves upstream with increasing values of U/U_r. Moreover, for all values of U/U_r, small-scale cells appear in the gap region of the slotted plate. These cells are characterized by the small-scale spiral patterns of streamlines; in many instances, they are connected to extensions of streamlines from the region of counterflow beneath the slotted plate.

The patterns of time-averaged vorticity $\langle \omega \rangle$ of Fig. 10 show, at all values of U/U_r, vorticity concentrations located in the gap region, and centered at an elevation corresponding to the upper edge of the slotted plate. The scale of these concentrations increases with increasing U/U_r.

The layout of Fig. 10 can be considered in parallel with Fig. 6, which represents the case of free-shear flow. Comparison of corresponding images for these two cases emphasizes the distinctive features of the shear flow past the slotted plate. In Fig. 6, the large-scale recirculation cell within the cavity is in the clockwise direction, as opposed to the counterclockwise pattern for all cases of the shear flow past the slotted plate. Furthermore, for the free-shear layer of Fig. 6, the time-averaged layer of vorticity is deflected downward into the cavity at the largest values of U/U_r. On the other hand, for the shear flow along the slotted plate, such downward deflection is precluded and the averaged pattern of vorticity $\langle \omega \rangle$ remains essentially horizontal with embedded concentrations of small-scale vorticity.

5.2. Instantaneous flow structure

The instantaneous structure of the shear flow along the slotted plate, and the recirculation flow below it, are indicated in the layout of Fig. 11, again for successively larger values of velocity $U/U_r = 0.56$, 0.74 and 1.00. The phase reference for this case is the same as for the images of Fig. 7: appearance of a cluster of instantaneous vorticity ω at a location immediately upstream of the impingement edge. Consider the patterns of instantaneous velocity V/U. For increasing values of U/U_r, the upward-oriented flow through the gaps of the slotted plate penetrates further into the shear layer above the plate. This general effect is also evident in the patterns of V'/U; at the highest value $U/U_r = 1.00$, the vectors have a substantial vertical component for a significant distance above the plate. An additional, common feature of all of the patterns of V'/U is the tendency to form a swirl-like region above the plate. The center of this swirl is at an elevation increasingly above the plate for larger values of U/U_r. The centers of each of these swirl patterns are approximately coincident with the centers of the large-scale clusters of vorticity ω formed above the plate. These clusters take on an elongated form at the lowest values of $U/U_r = 0.56$ and 0.74 and become increasingly concentrated at $U/U_r = 1.00$. It is therefore evident that an instability mechanism promotes the agglomeration of vorticity with increasing streamwise distance along the plate. Furthermore, patterns of coherent velocity correlation $u'v'/U^2$ are evident along the upper surface of the slotted plate for higher values of $U/U_r = 0.74$ and 1.00. The centers of these coherent regions tend to occur along the trailing region of the large-scale cluster of vorticity ω and, furthermore, both the spatial extent and the peak values of $u'v'/U^2$ increase with increasing U/U_r. These peak values of $u'v'/U^2$ are -0.014, -0.051 and -0.059 respectively for values of $U/U_r = 0.56$, 0.74 and 1.00.

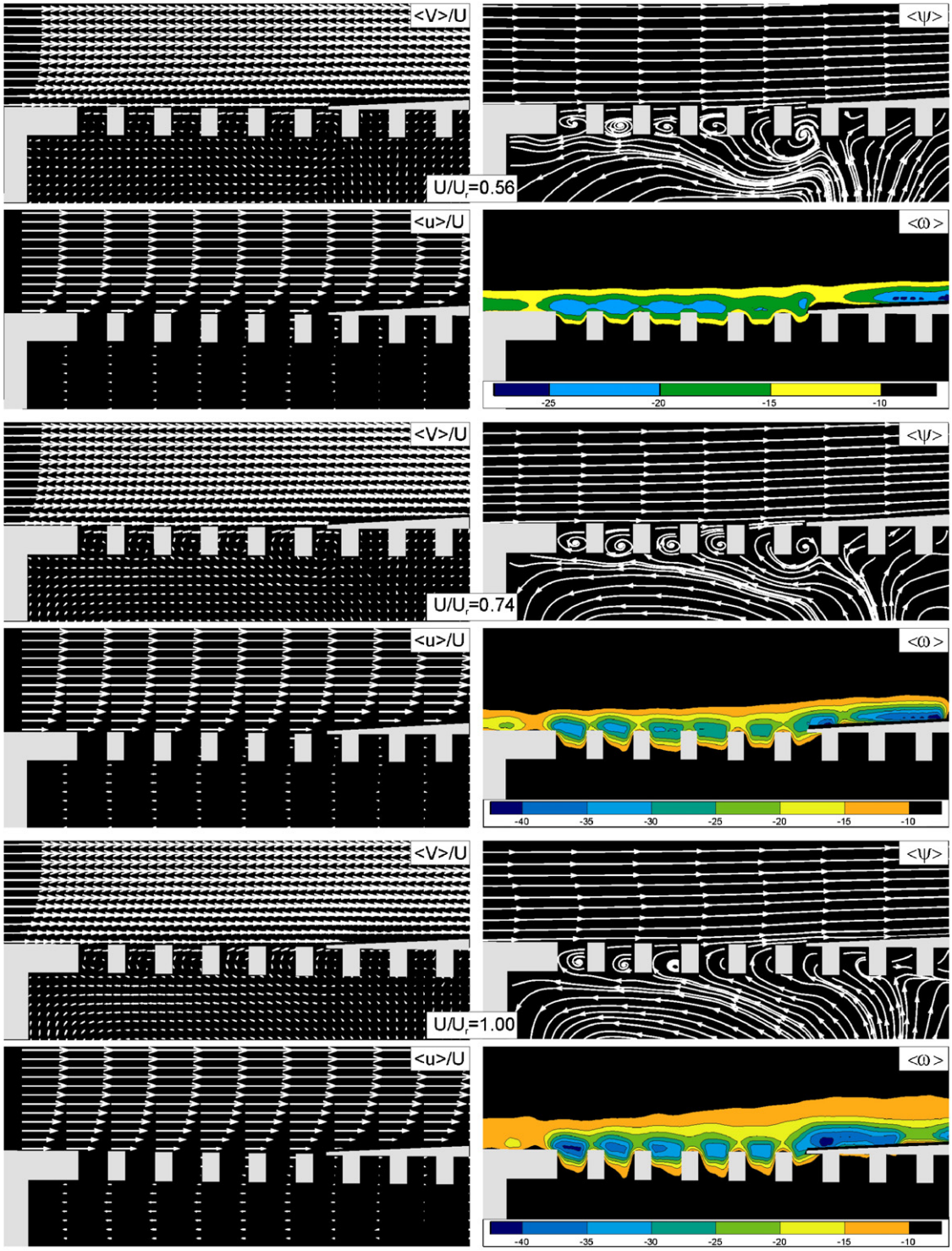

Fig. 10. Comparison of time-averaged patterns of velocity $\langle V \rangle / U$, streamwise component of velocity $\langle u \rangle / U$, streamlines $\langle \Psi \rangle$ and vorticity $\langle \omega \rangle$. Images are shown for three different values of velocity ratio U/U_r, which represents the ratio of the free-stream velocity U to its value U_r at the resonance condition in presence of the slotted plate. For the patterns of vorticity, the minimum and incremental values are $|\omega|_{\min} = 10$ and $|\Delta\omega| = 5\,\mathrm{s}^{-1}$. The zeroth level and the first levels above and below zero are omitted for the clearer illustration of the flow structure.

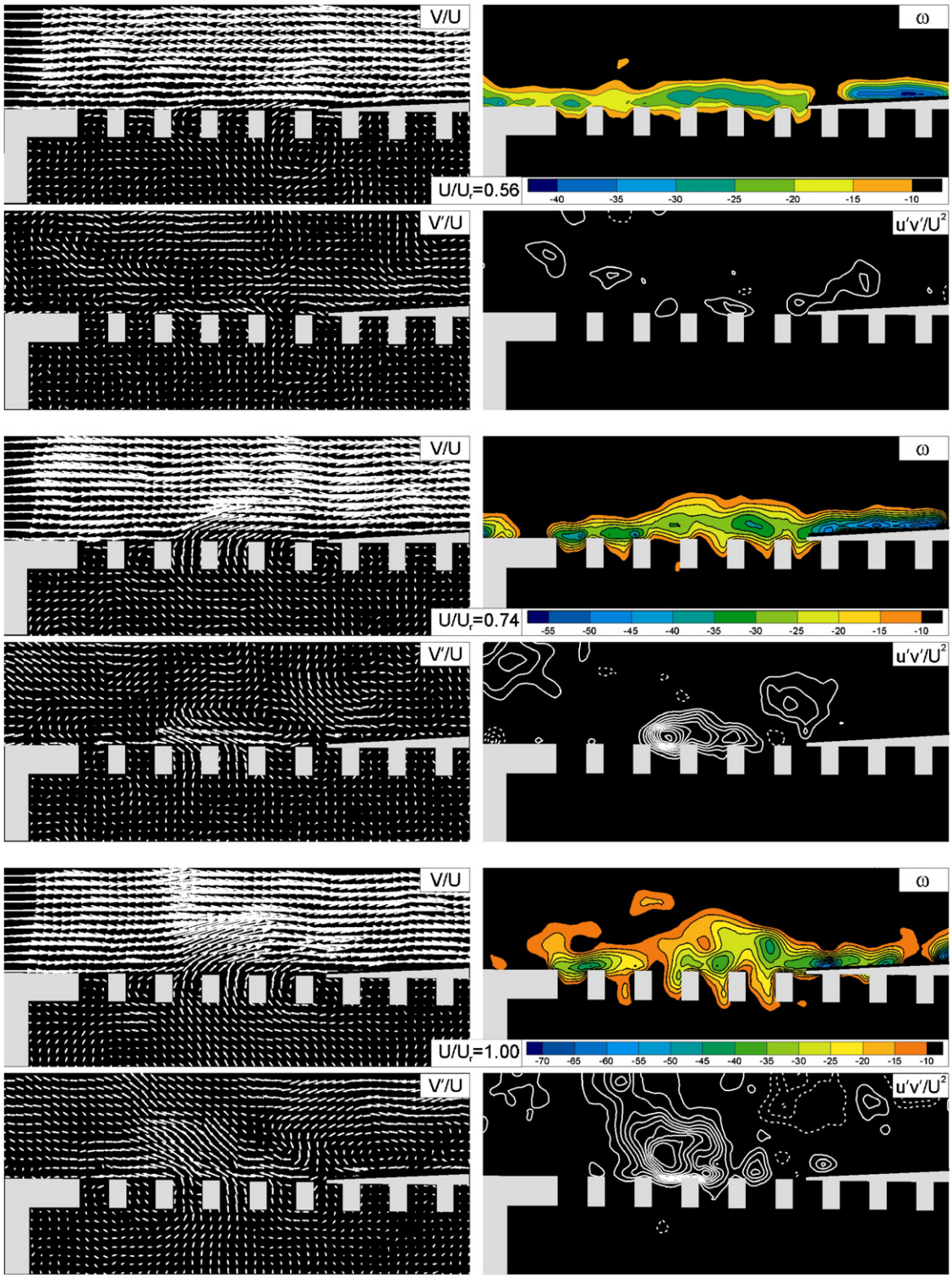

Fig. 11. Patterns of instantaneous velocity V/U, velocity fluctuation V'/U, vorticity ω and velocity correlation $u'v'/U^2$ for three values of the ratio of free-steam velocity U to its value U_r at the resonance condition, in presence of the slotted plate. For patterns of vorticity, the minimum and incremental values are $|\omega|_{\min} = 10$ and $|\Delta\omega| = 5\,\mathrm{s}^{-1}$. For the contours of constant velocity correlation, the minimum and incremental values are $|[u'v'/U^2]|_{\min} = 0.005$ and $|\Delta[u'v'/U^2]| = 0.005$; solid lines are negative and dashed lines are positive values. Images at $U/U_r = 1.00$ are from Ekmekci and Rockwell (2003).

The foregoing features of the instantaneous structure of the shear layer along the plate shown in Fig. 11, relative to the structure of the free-shear layer in Fig. 7, reveal the following distinctions. Regarding the patterns of instantaneous velocity V/U, both cases show pronounced, upward ejection of fluid from the cavity to the region of shear flow above the cavity opening. The magnitude and degree of penetration of this upward-oriented flow is, however, inhibited by presence of the slotted plate. In fact, this general observation occurs for all values of U/U_r. A similar observation holds for the patterns of V'/U.

Concerning the patterns of instantaneous vorticity ω of Fig. 11, the spatial extent, i.e., scale, of the large-scale cluster of vorticity, is larger for the free-shear layer in absence of the plate as shown in Fig. 7. The peak values of vorticity ω are approximately the same for both cases.

Finally, the patterns of instantaneous velocity correlation $u'v'/U^2$ are more extensive over the spatial domain and have substantially higher peak values for the free-shear layer of Fig. 7, relative to those of Fig. 11. It is evident that presence of the plate slats significantly inhibits the correlation between the fluctuations u' and v'; nevertheless, this correlation has sufficiently high values at larger ratios of U/U_r in presence of the slotted plate to allow existence of a coherent oscillation.

5.3. Time traces and spectra

Additional features of the unsteady flow field past the slotted plate are represented by the patterns of Fig. 12, which shows autospectral density contours $|S_u(f_o)|$ at the predominant frequency f_o for the same values of $U/U_r = 0.56$, 0.74 and 1.00 as in the foregoing. (The units of $S_u(f)$ are mm/s.) For increasing values of U/U_r, the peak amplitudes of the autospectral density increase in the region immediately above the surface of the plate and, moreover, significant values arise in the region below the plate. The corresponding time traces and autospectral density of the longitudinal u component are shown at locations a, b and c. These representations indicate that the fluctuations are generally more organized and have larger peak amplitudes for the region above the plate. Furthermore, the degree of organization, or coherence of these oscillations, increases with increasing U/U_r. These features, more specifically the cases $U/U_r = 0.56$ and 1.00, were reported in the preliminary investigation of Ekmekci and Rockwell (2003).

The foregoing observations show significant differences relative to the case of the free-shear flow addressed in Fig. 8. The most significant difference concerns the fluctuations at location b, which is within the resonant cavity. In absence of the plate (Fig. 8), these fluctuations can have the same degree of organization and nearly the same magnitude as those in the shear layer above the cavity opening, represented by points a and c. This observation emphasizes the globally coupled phenomenon of the free-shear layer (no plate)–resonant cavity interaction. Although significant global coupling may occur in presence of the slotted plate, it is evident that the fluctuating activity within the resonant cavity is inhibited.

5.4. Time averaged representations of the fluctuating flow structure

Fig. 13 gives patterns of the time-averaged fluctuating quantities, which include the transverse velocity fluctuation v_{rms}/U, longitudinal component u_{rms}/U, the Reynolds stress correlation $\langle u'v' \rangle/U^2$ and the phase angle $\Phi_u(f_o)$ at the predominant frequency f_o. The patterns of v_{rms}/U show increasingly larger fluctuation amplitudes in the gap region between the slats for increasing values of U/U_r. In fact, considering the entire domain above and below the slotted plate, peak values of v_{rms}/U always occur in the gap region between the slats. Regarding the patterns of longitudinal fluctuation u_{rms}/U, peak values occur along the upper edge of the slotted plate for all values of U/U_r. These peak values are $v_{rms}/U = 0.056$, 0.069, 0.103 and $u_{rms}/U = 0.201$, 0.219 and 0.214 respectively for values of $U/U_r = 0.56$, 0.74 and 1.00. Furthermore, the region beneath the plate shows increasingly larger values of u_{rms}/U for increasing values of U/U_r.

Regarding the correlations $\langle u'v' \rangle/U^2$, both their spatial extent and their peak magnitudes increase with increasing values of U/U_r. The peak values of $\langle u'v' \rangle/U^2 = -0.005$, -0.010 and -0.015 are determined, respectively, for values of $U/U_r = 0.56$, 0.74 and 1.00. In fact, these peak values tend to occur at the centers of the cell-like concentrations of $\langle u'v' \rangle/U^2$.

Corresponding patterns of phase angle $\Phi_u(f_o)$ at the predominant frequency of oscillation f_o are shown in the right column of Fig. 13. At the lowest value of velocity, $U/U_r = 0.56$, where the oscillation has relatively low amplitude and does not exhibit significant coupling with the resonant mode of the cavity, the patterns of $\Phi_u(f_o)$ show a number of small-scale irregularities. At larger values of $U/U_r = 0.74$ and 1.00, these irregularities disappear, as the oscillation becomes more coherent and of larger amplitude. At the elevation above the slotted plate, corresponding to the white dot, it is, however, possible to define a well-defined continuous variation of the phase $\Phi_u(f_o)$, as a function of streamwise

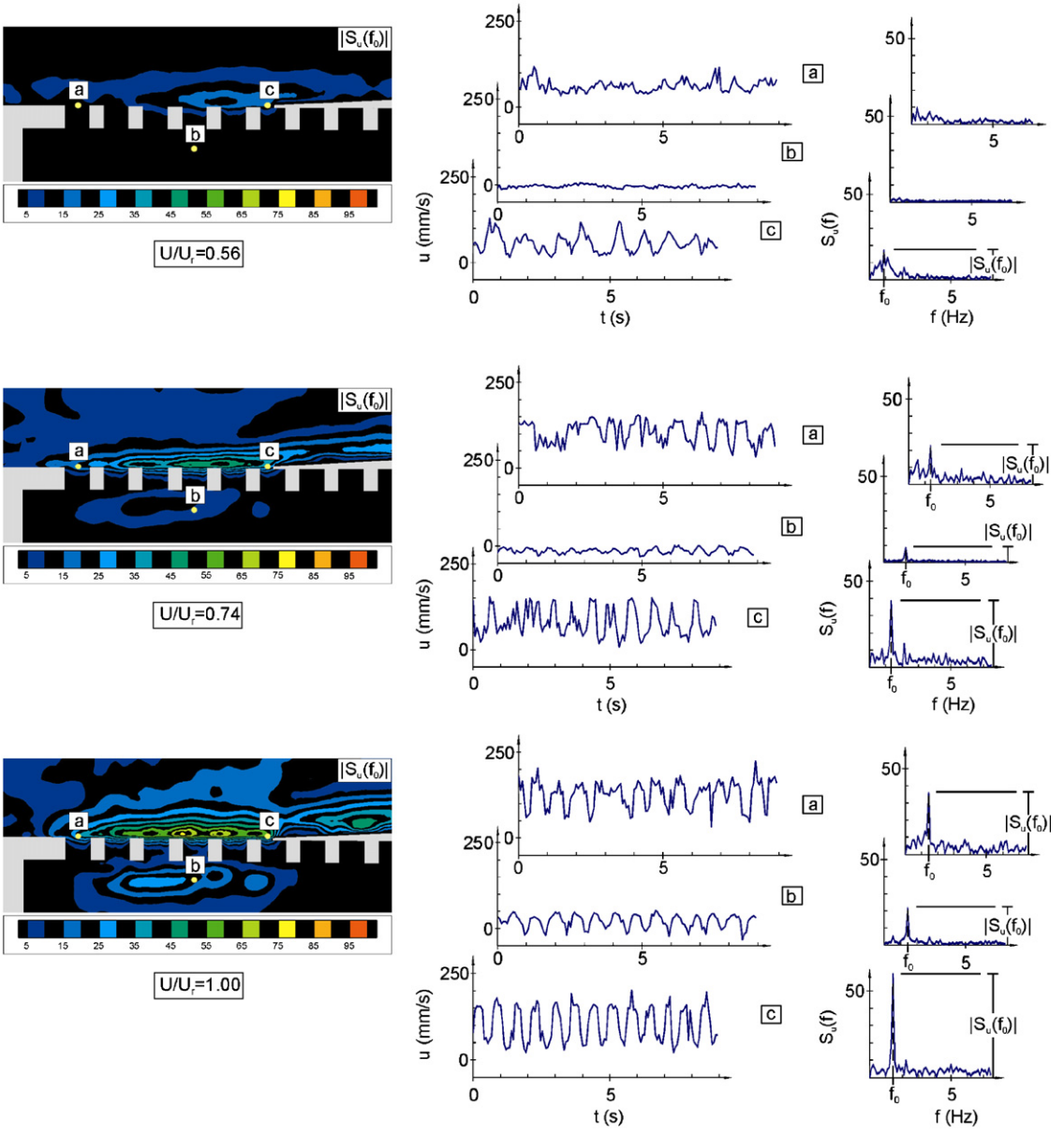

Fig. 12. Images showing contours of constant peak amplitude of autospectral density $|S_u(f_o)|$ of fluctuating streamwise velocity u at predominant frequency f_o and representative values of time traces of streamwise velocity u and spectra $S_u(f)$ in presence of the slotted plate. These images and plots are shown for three values of velocity ratio U/U_r, in which U is the free-stream velocity and U_r corresponds to its value at the resonance condition. Minimum and incremental values are $[|S_u(f_o)|]_{\min} = 5$ and $\Delta[|S_u(f_o)|] = 5$. Cases $U/U_r = 0.56$ and 1.00 are from Ekmekci and Rockwell (2003).

distance. This distribution of phase, as well as the overall phase difference, exhibits ordered values with increasing U/U_r, as will be illustrated in Fig. 14.

Comparison of the aforementioned features of the averaged fluctuation fields of the shear layer along the plate (Fig. 13) with those of the free-shear in absence of the plate (Fig. 9) reveal the following differences. For the free-shear layer, the patterns of both v_{rms}/U and u_{rms}/U show a single, large-scale form; it is centered approximately at the elevation of the inflection point of the averaged shear layer (compare velocity profiles of Fig. 6) for the v_{rms}/U distributions. For the u_{rms}/U distributions, it is centered along the line extending from the leading-corner of the cavity. In contrast, the presence of the plate induces a number of maxima of v_{rms}/U and u_{rms}/U between, and along, the upper edges of the slats.

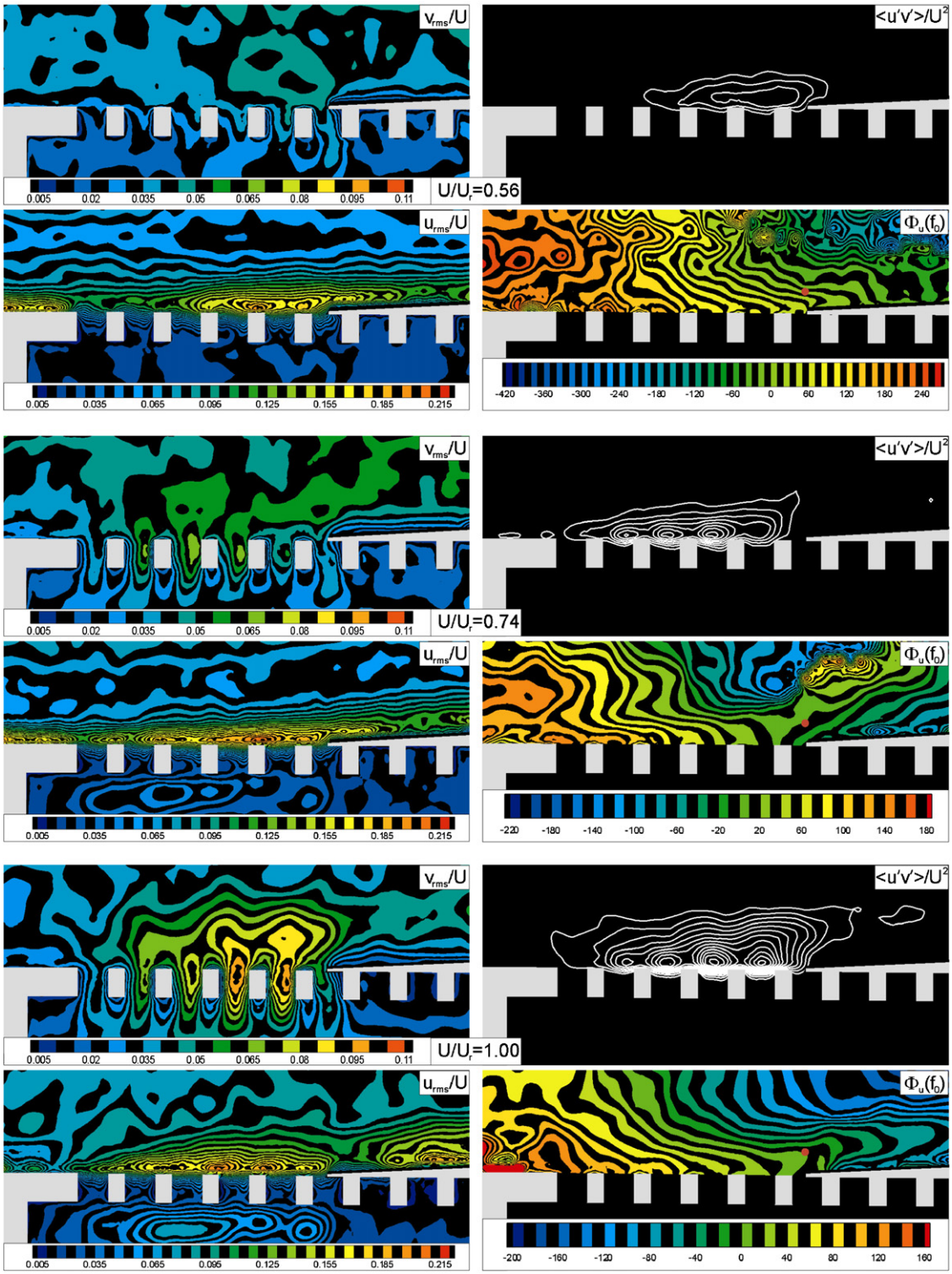

Fig. 13. Contours of constant transverse velocity fluctuation $v_{\rm rms}/U$, longitudinal velocity fluctuation $u_{\rm rms}/U$, Reynolds stress correlation $\langle u'v'\rangle/U^2$ and phase angle $\Phi_u(f_o)$ at predominant frequency, f_o, for three different values of U/U_r, in which U is the free-stream velocity and U_r is its value at the resonance condition in presence of the slotted plate. Minimum and incremental values of $v_{\rm rms}/U$ are $[v_{\rm rms}/U]_{\rm min} = 0.005$ and $\Delta[v_{\rm rms}/U] = 0.005$. For longitudinal velocity fluctuation $u_{\rm rms}/U$, minimum and incremental values are $[u_{\rm rms}/U]_{\rm min} = 0.005$ and $\Delta[u_{\rm rms}/U] = 0.005$. For velocity correlation, $\langle u'v'\rangle/U^2$, minimum and incremental values are $|[\langle u'v'\rangle/U^2\rangle]|_{\rm min} = 0.002$ and $|\Delta[\langle u'v'\rangle/U^2]| = 0.001$; solid lines show negative values.

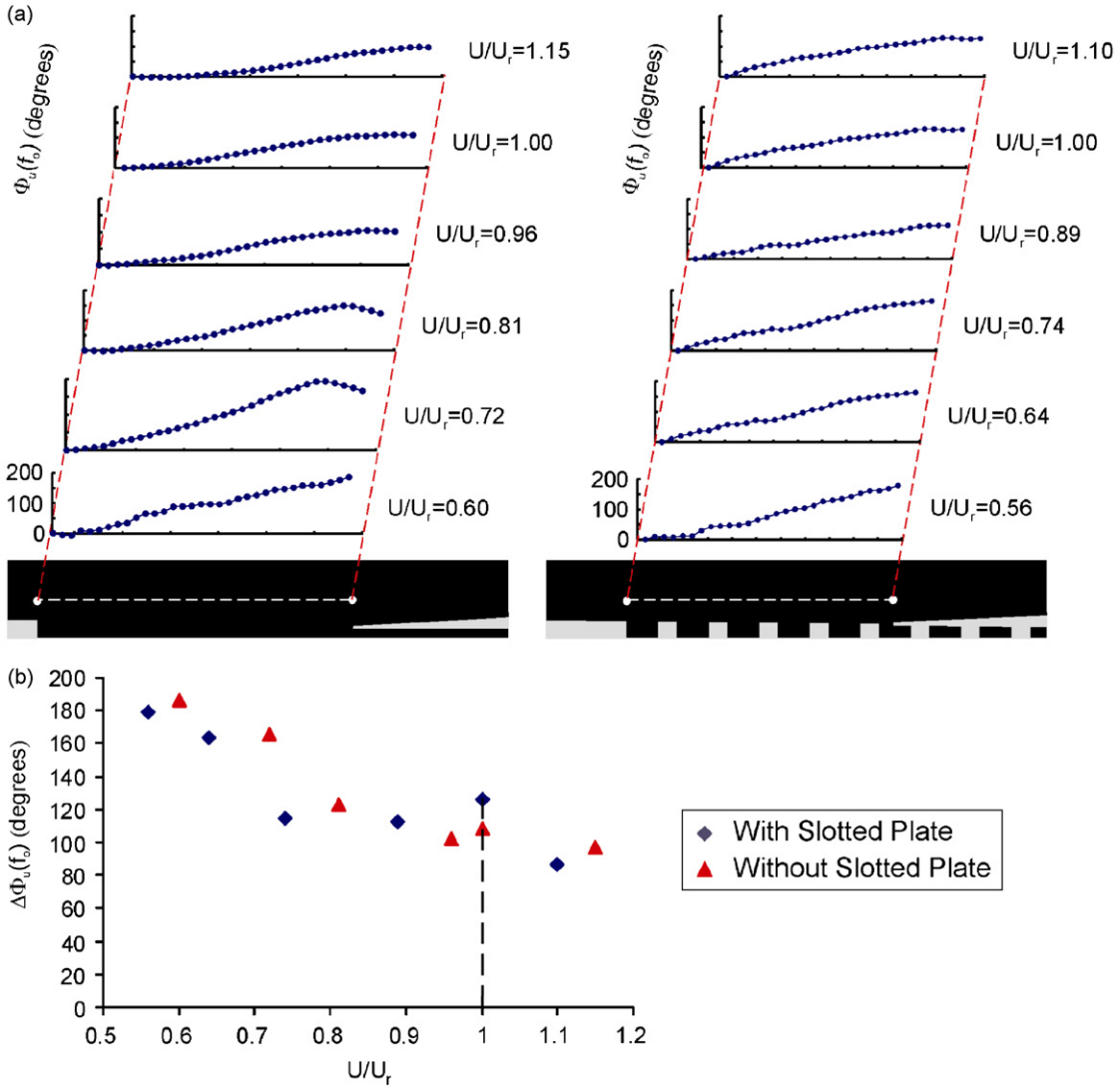

Fig. 14. (a) Variation of local value of phase $\Phi_u(f_o)$ with distance from separation to impingement; and (b) phase difference $\Delta\Phi_u(f_o)$ between separation and impingement versus U/U_r.

Finally, the patterns of Reynolds stress correlation $\langle u'v' \rangle / U^2$ for the free-shear layer (Fig. 9) have a much larger spatial extent and larger peak values than those in presence of the plate (Fig. 13). These patterns of high $\langle u'v' \rangle / U^2$ extend across the shear layer and well down into the cavity for the case of the free-shear layer. On the other hand, for the shear layer along the plate, significant correlations $\langle u'v' \rangle / U^2$ exist only in the region above the plate for the bounded shear layer.

Regarding the contours of constant phase angle $\Phi_u(f_o)$ for cases of the free-shear layer (Fig. 9) and the shear layer along the bounding plate (Fig. 13), the following similarities are evident. At the lowest value of U/U_r, for which coupled oscillations do not occur, small-scale irregularities occur in the upper region of the flow, where the fluctuation amplitudes are small and the degree of coherence is low. At a representative elevation above the impingement plate, however, relatively smooth and continuous variations of phase are observable, and can reliably indicate the streamwise variation of phase, as well as the overall phase difference between separation and impingement of the shear flow. At higher values of U/U_r, extending up to a value of 1.00, the phase distributions, for both the free-shear layer and the shear layer along the plate, show well-defined, continuous variations. In all of these cases, the lines of constant phase take the form of an inclined pattern at an elevation above the impingement edge, which indicates that substantial phase

gradients exist across the shear layer at a given streamwise distance. The general similarity of these patterns in Figs. 6 and 10, at sufficiently large values of U/U_r, is in accord with similar streamwise distributions of phase $\Phi_u(f_o)$, as addressed in the next section.

6. Streamwise phase variations along oscillating shear layer

The cross-spectrum of the u component of the velocity fluctuation was evaluated at a grid size of $0.03L$ over the entire domain of a given image, in which L is the impingement distance between the leading-corner of the cavity and the tip of the impingement edge. Values of phase $\Phi_u(f_o)$ were then determined and plotted along a line at a reference elevation in the shear layer, indicated by the horizontal white-line of Fig. 14(a). These variations of phase $\Phi_u(f_o)$ show well-defined increases with streamwise distance.

It is evident for cases of both the free-shear layer and the shear layer along the plate, that the overall form of these phase variations is remarkably similar and, furthermore, the overall phase difference $\Delta\Phi_u(f_o)$ between the leading-corner of the cavity and the impingement edge tip, shown in Fig. 14(b), is approximately the same for these extreme cases. This overall phase difference $\Delta\Phi_u(f_o)$ is plotted as a function of the velocity ratio U/U_r. The trend of the data points is remarkably similar for both cases, which suggests that the mechanisms of the onset of complete resonant coupling are similar. At the lowest value of U/U_r, in the range 0.5–0.6, the overall phase shift $\Delta\Phi_u(f_o)$ has a value of approximately 180°. With increasing U/U_r, this phase difference decreases until at resonance, represented by $U/U_r = 1.0$, the value of phase shift is of the order of 120°.

Although the streamwise variation of phase of the velocity fluctuation is the same for both the cases of the free shear layer and the shear layer along the slotted plate, the values of U_r at which a fully locked-on, resonant-coupled oscillation occurs is different. The Strouhal numbers f_rL/U for the free-shear layer and the shear layer along the slotted plate are different as well and have values of 0.32 and 0.24. Physically, this distinction is due to the different phase speeds of the instabilities of the free shear layer and the shear layer along the slotted plate.

7. Oscillations of shear layer along a slotted plate in presence of a resonant cavity: effect of plate geometry

For the aforementioned comparisons between oscillations of the free-shear layer and the shear layer along the slotted plate, the plate geometry was selected on the basis of preliminary diagnostics. This particular geometry yielded highly coherent oscillations, as described in the preceding sections. The issue arises as to how the thickness w of the individual slats and the gap width G between slats influence the onset of self-sustained oscillations. For our present considerations, the gap distance G and the slat thickness w are expressed in normalized form as $G^* = G/\theta$ and $w^* = w/\theta$, in which θ is the momentum thickness of the inflow boundary layer.

Fig. 15 shows time-averaged patterns of Reynolds stress correlation $\langle u'v' \rangle / U^2$, contours of constant peak amplitude $|S_u(f_o)|$ of the autospectral density, and time traces and spectra of longitudinal fluctuation u at the location of the peak value of the correlation $\langle u'v' \rangle / U^2$. The location of this peak is represented by the dot on the contours of constant $\langle u'v' \rangle / U^2$. It is evident that values of gap width $G^* = 2.5$ give rise to pronounced oscillations, even when the thickness w^* is varied over the range 0.5–1.5. The largest amplitude oscillation occurs for the thinnest slat $w^* = 0.5$, represented by the first row of images. Successive increases in the value of thickness w^*, as indicated by the second and third row of images, result in a discernible decrease in the peak amplitude.

If the gap width is increased to a value of $G^* = 5.0$, the amplitude of the peak in the spectrum $S_u(f)$ decreases substantially to a value of approximately one-half that of the foregoing values. In addition, it is evident from the time trace that the degree of organization of fluctuation is significantly reduced.

Further representations of the effect of thickness w^* and gap G^* are given in the right column of images in Fig. 15, which shows contours of constant peak amplitude $|S_u(f_o)|$ of the autospectral density. In all cases, the peak amplitudes occur in the region immediately above the plate. Discernible contours are, however, evident in the cavity immediately beneath the plate. The largest peak amplitudes in this region occur for the thinnest slats, $w^* = 0.5$ and 1.0.

Fig. 15. Contours of time-averaged Reynolds stress correlation $\langle u'v' \rangle / U^2$ and constant amplitude of autospectral density $|S_u(f_o)|$ of fluctuating streamwise velocity u at predominant frequency f_o for various values of dimensionless slat thickness w^* and gap width G^* between slats of the slotted plate, in which $w^* = w/\theta$ and $G^* = G/\theta$, where θ is the inflow momentum thickness. Also illustrated are time traces of longitudinal velocity fluctuation $u(t)$ and autospectral density $S_u(f)$ at the location of the maximum value of correlation $\langle u'v' \rangle / U^2$ (see location of dot in each image). For velocity correlation, $\langle u'v' \rangle / U^2$, minimum and incremental values are $|[\langle u'v' \rangle / U^2]|_{\min} = 0.002$ and $|\Delta[\langle u'v' \rangle / U^2]| = 0.001$; solid lines show negative values. For amplitude of autospectral density, $|S_u(f_o)|$, minimum and incremental values are $[|S_u(f_o)|]_{\min} = 5$ and $\Delta[|S_u(f_o)|] = 5$.

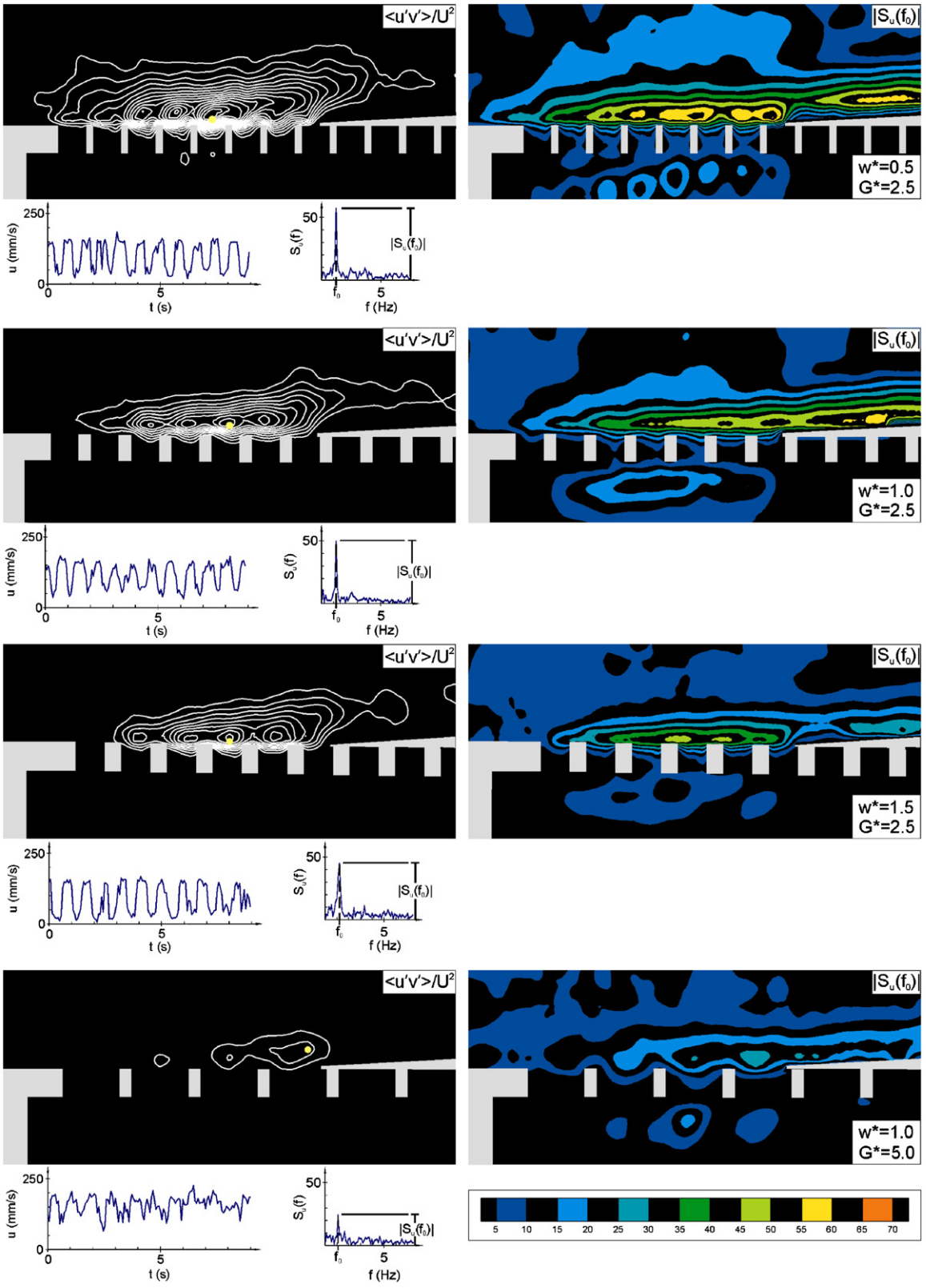
<u'v'>/U²
|S_u(f_0)|
w*=0.5
G*=2.5
u (mm/s)
t (s)
S_u(f)
f (Hz)
w*=1.0
G*=2.5
w*=1.5
G*=2.5
w*=1.0
G*=5.0
5 10 15 20 25 30 35 40 45 50 55 60 65 70

Furthermore, this pattern corresponding to $w^* = 0.5$ takes the form of spatially periodic contours, in accord with the gap G^*, whereas for larger values of slat thickness w^*, this small-scale spatial periodicity does not occur.

Fig. 16 shows the structure of shear layer past the slotted plate, represented by patterns of instantaneous velocity vectors V and vorticity ω. The values of dimensionless plate thickness w^* and gap width G^* are the same as in Fig. 15. Each of the instantaneous patterns of Fig. 16 was selected from the sequence of images according to the following criterion: appearance of a cluster of instantaneous vorticity ω at a location immediately upstream of the impingement edge. Among the plate geometries having the smallest gap width $G^* = 2.5$, represented by the first through third row of images, the plate with the thinnest slat $w^* = 0.5$ shows the furthest vertical penetration of the ejected flow from the cavity into the shear layer along the upper side of the plate. As the slat thickness w^* increases, penetration of this jet-like flow decreases. This vertical ejection of flow is closely associated with the mechanism that allows the cavity fluctuations to trigger the development of pronounced oscillations in the shear layer. It appears that the subtle increases in slat thickness w^*, observed in Fig. 15, gradually inhibit this ejected flow. The increase in gap width to a value of $G^* = 5.0$, shown in the fourth row of images of Fig. 16, further inhibits the penetration from the cavity to shear layer region.

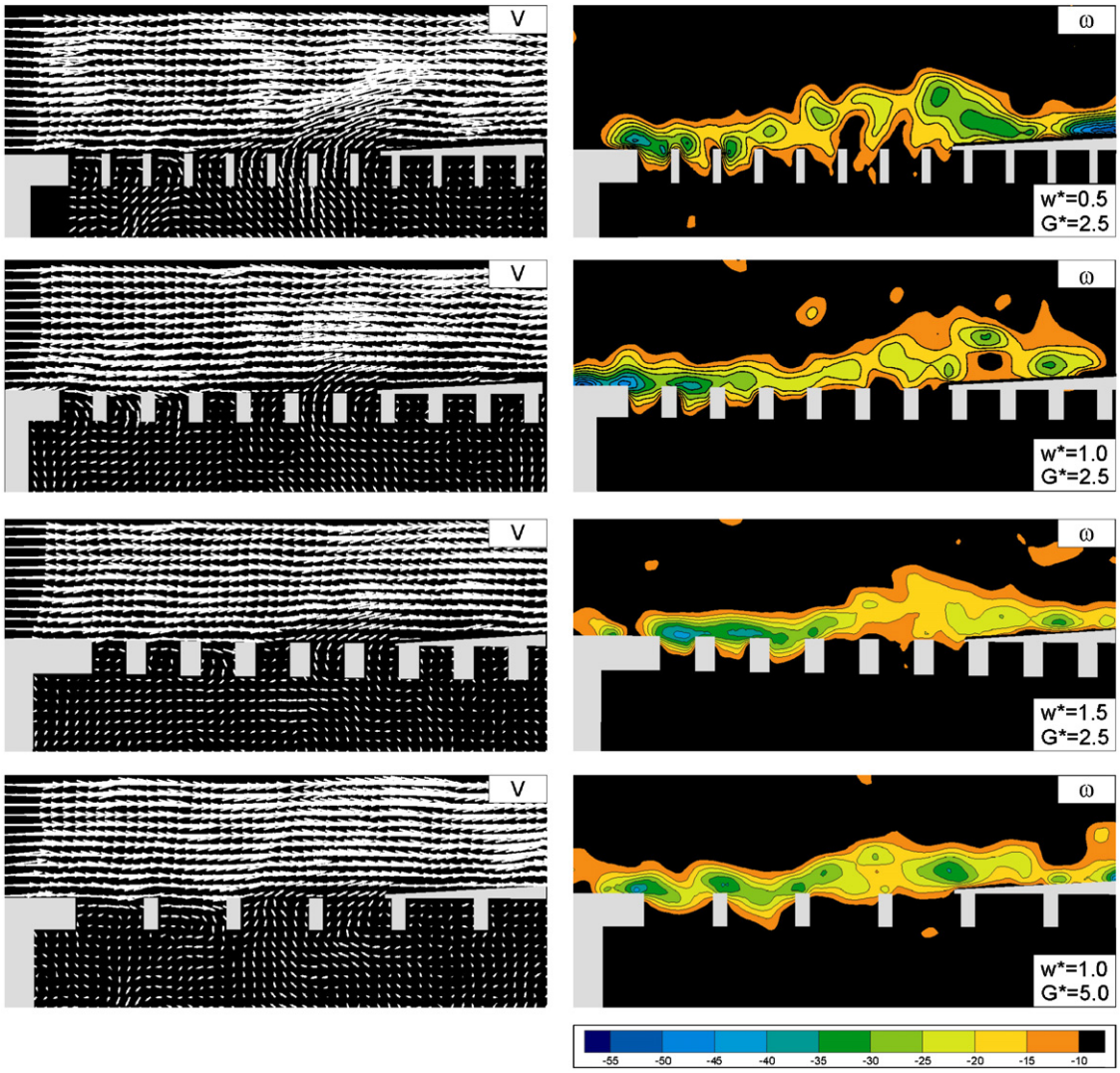

Fig. 16. Patterns of instantaneous velocity V and vorticity ω for various values of dimensionless plate thickness w^* and gap width G^* between slats of slotted plate, in which $w^* = w/\theta$ and $G^* = G/\theta$, where θ is the inflow momentum thickness. For vorticity, minimum and incremental values are $|\omega|_{\min} = 10$ and $|\Delta\omega| = 5\,s^{-1}$.

A decrease in the degree of coherency of the fluctuating flow field occurs, as represented by the contours of Reynolds stress $\langle u'v' \rangle / U^2$.

Contours of constant phase $\Phi_u(f_o)$ at the oscillation frequency f_o are shown in Fig. 17; they are calculated from the cross-spectrum at each grid point; the reference point is designated by the dot above the impingement edge. Along the top edge of the slats, these contours are locally distorted, but at a slightly higher elevation, the phase indicates an ordered variation in the streamwise direction, except for the largest value of $G^* = 5.0$, for which oscillations are attenuated; (compare to Fig. 15.) In other words, when the amplitude of oscillation is attenuated, the phase contours exhibit an increasing disorder, i.e., the onset of phase "jitter".

Time-averaged values of transverse velocity fluctuation v_{rms}/U and longitudinal velocity fluctuation u_{rms}/U are given respectively in the left and right columns of Fig. 18. Regarding the contours of constant v_{rms}/U, relatively large amplitude fluctuations occur within, above, and below the gaps for the parameters of the slotted plate corresponding to the first row of images. The peak amplitude of these fluctuations in the gap region decreases for the configurations shown in the second through fourth rows of images and, furthermore, there is significant drop-off of fluctuation amplitude in the regions above and below the slotted plate. These peak values are $v_{rms}/U = 0.1048$, 0.0816, 0.0711 at the smaller gap value $G^* = 2.5$ for values of $w^* = 0.5$, 1.0 and 1.5 and $v_{rms}/U = 0.0609$ at the largest gap $G^* = 5.0$ for the thickness $w^* = 1.0$.

For the case of the longitudinal (streamwise) velocity fluctuation u_{rms}, substantial magnitudes of dimensionless fluctuation u_{rms}/U occur along the upper edge of the slotted plate configuration. At smaller values of gap $G^* = 2.5$, these peak values are $u_{rms}/U = 0.2243$, 0.2129, and 0.2414 for values of $w^* = 0.5$, 1.0 and 1.5. At the largest gap $G^* = 5.0$, represented in the fourth row of images, these peak amplitudes decrease significantly to a value $u_{rms}/U = 0.1748$. In the region below the slotted plate, the patterns of u_{rms}/U closely follow the contours of constant autospectral density given in the right column of Fig. 15, due to the relatively high coherence of the oscillation.

8. Concluding remarks

The aim of the present investigation has been to characterize in detail the global, quantitative features of a shear layer-cavity system for states prior to and at the onset of fully coupled resonant oscillations. In parallel with this effort, a central thrust was to determine the distinctive features of the onset of oscillation for the case of a free-shear flow along the cavity opening, relative to shear flow past a slotted plate along the opening. The primary features are addressed in the following:

Onset of fully coupled resonant oscillation of unstable shear flow. The two cases of the free-shear flow and the shear flow along the slotted plate exhibit remarkably similar variations of dimensionless frequency as the dimensionless velocity approaches the fully coupled resonant conditions. This observation indicates that an inherent hydrodynamic instability of both the free-shear flow and the shear layer on a slotted plate exist, as an essential ingredient, for the resonant coupling mechanism. The existence of the former instability is well known.

Onset of resonance: Development of instantaneous patterns of large-scale vorticity. For cases of both the free-shear layer and the shear layer along the slotted plate, prior to the onset of resonant coupling with the cavity, the vorticity layer takes on a small-scale, highly elongated form, and as the fully coupled resonant state is approached, both the peak vorticity and the scale of the vorticity cluster increase. The effect of the slotted plate is, however, to decrease the spatial extent and circulation of the large-scale pattern of vorticity; this circulation is approximately one-half that of the corresponding free-shear layer at the onset of resonant coupling.

Onset of resonance: Instantaneous correlations of unsteady velocity field. The peak amplitude and spatial extent of patterns of $u'v'$ can be employed as an indicator of the degree of lock-on of the oscillating shear layer, both for the case of the free-shear layer and the shear layer along the slotted plate. Large-scale clusters of $u'v'$ occur for both classes of shear flows and are associated with large amplitude, vertical ejections of fluid from the cavity into the high-speed region of the shear layer; for the shear layer along the slotted plate, the peak magnitudes of $u'v'$ are of the order of one-third those of the free-shear layer at the onset of resonant coupling.

Onset of resonance: Time-averaged patterns of fluctuations. For the case of the free-shear layer, single, large-scale clusters of the patterns of v_{rms} and u_{rms} are evident; their peak magnitude and spatial location are directly related to the degree of resonant coupling. For the case of the shear layer past the slotted plate, small-scale concentrations of v_{rms} occur in the gap regions of the slats and a small-scale cluster of u_{rms} exists along the upper edge of the slotted plate. The peak magnitudes of these small-scale clusters of u_{rms} and v_{rms} increase as the degree of lock-on increases. Thus, despite the remarkable similarity of other indicators of the onset of lock-on, such as variation of dimensionless frequency over the range of dimensionless velocity, the onset and evolution of large-scale clusters of vorticity ω and velocity correlation

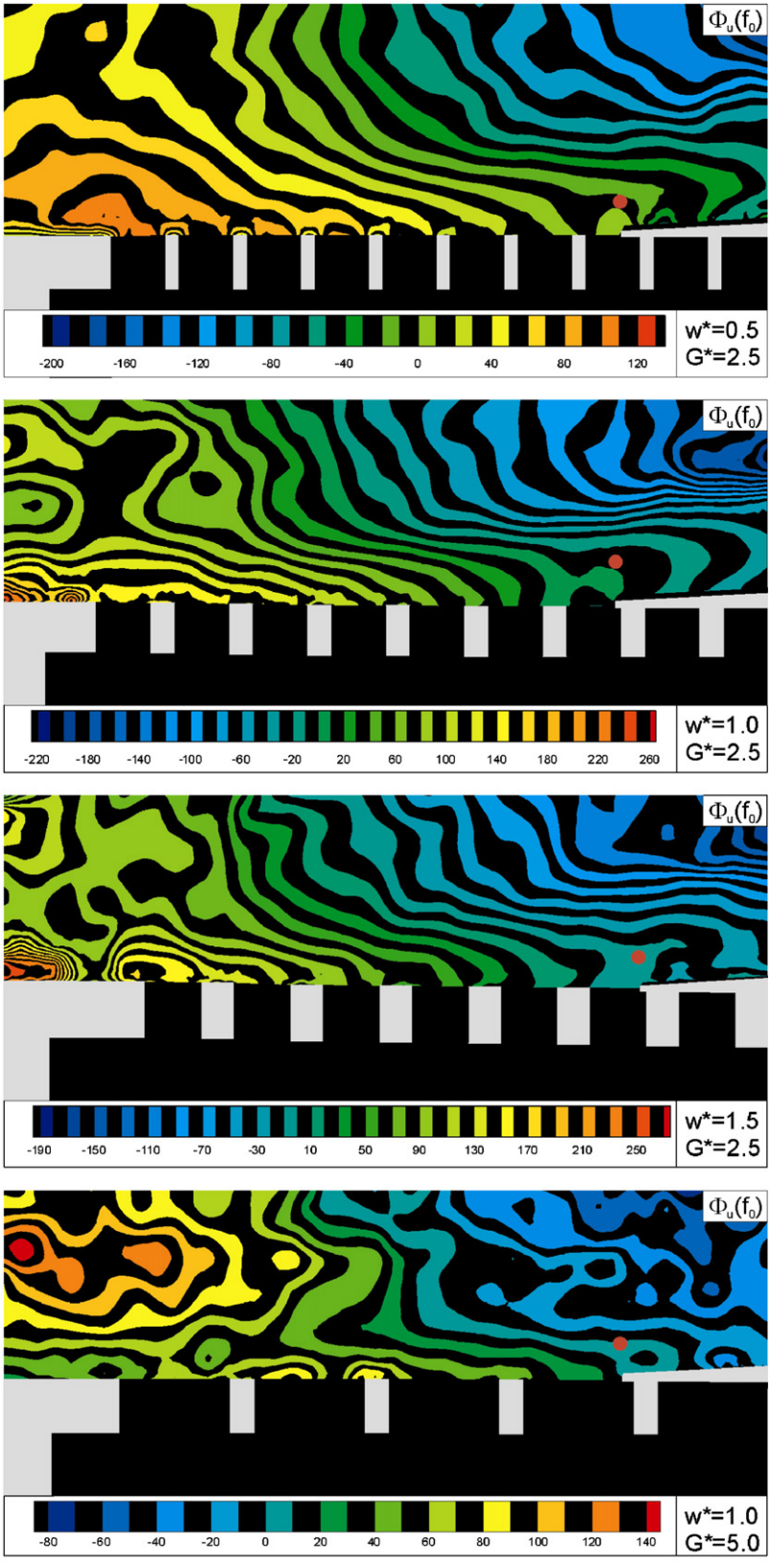

Fig. 17. Contours of constant phase angle $\Phi_u(f_o)$ of the longitudinal velocity fluctuation at predominant frequency, f_o, for various values of dimensionless thickness w^* of the slats and gap width G^* between slats of the slotted plate, in which $w^* = w/\theta$ and $G^* = G/\theta$, where θ is the inflow momentum thickness.

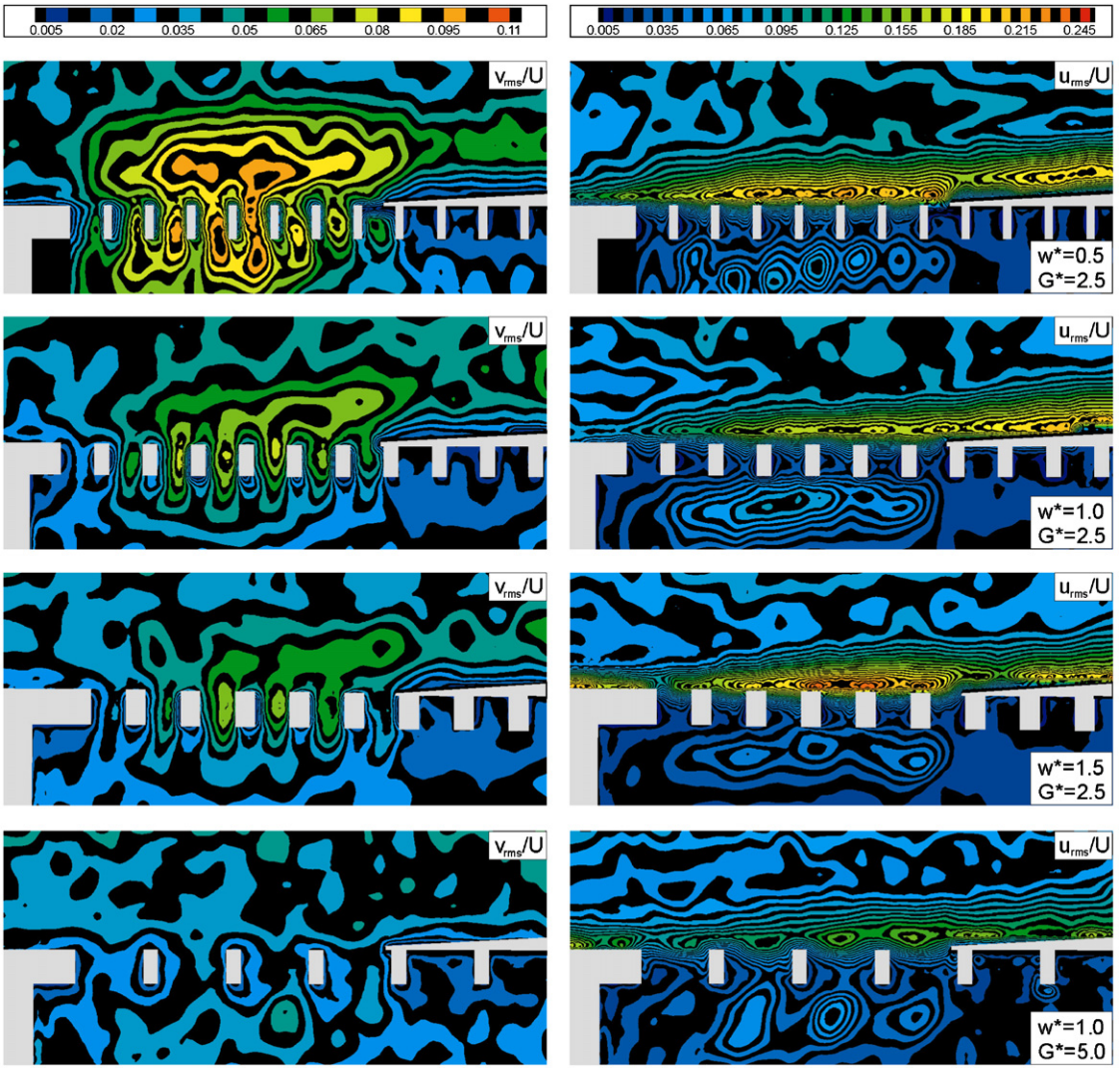

Fig. 18. Contours of constant transverse velocity fluctuation v_{rms}/U and longitudinal velocity fluctuation u_{rms}/U for various values of dimensionless thickness w^* of the slats and gap width G^* between the slats of the slotted plate, in which $w^* = w/\theta$ and $G^* = G/\theta$, where θ is the inflow momentum thickness. Minimum and incremental values of v_{rms}/U are $[v_{\mathrm{rms}}/U]_{\mathrm{min}} = 0.005$ and $\Delta[v_{\mathrm{rms}}/U] = 0.005$. For longitudinal velocity fluctuation, u_{rms}/U, $[u_{\mathrm{rms}}/U]_{\mathrm{min}} = 0.005$ and $\Delta[u_{\mathrm{rms}}/U] = 0.005$.

$u'v'$, for the free-shear layer and the shear layer along the slotted plate, the patterns of v_{rms} and u_{rms} are fundamentally different for these two cases.

Onset of resonance: Phase variations along the cavity shear layer. Patterns of phase contours $\Phi_u(f_o)$ show, for both the free-shear layer and the shear layer along the slotted plate, increasing coherence, of a similar form, as the degree of locked-on resonant coupling increases. Furthermore, the overall phase difference, between the locations of separation and impingement, is of the order of π for the case of insignificant resonant coupling and $2\pi/3$ for fully coupled oscillations.

Onset of resonance: Role of recirculation zone within cavity. For the oscillations of the free-shear layer along the cavity, a large-scale (clockwise) recirculation cell exists, in order to satisfy the entrainment demands of the developing shear layer along the cavity. In contrast, for the case of the shear layer along the slotted plate, a counter-clockwise recirculation cell is induced. It is apparently associated with the flow pulsations through individual slats. The streamlines of this large-scale cell connect to small-scale cells that exist within the gaps of the slotted plate.

Onset of resonance: Effect of geometry of slotted plate. Highly coherent oscillations, coupled with the resonant mode of the cavity, are attainable for a range of gap width and thickness of individual slats in the slotted plate. When an optimal value of gap is attained, a three-fold range of slat thickness can still lead to a highly organized oscillation. In the limiting case of a sufficiently large gap, however, the degree of organization and thereby the amplitude of the resonant-coupled oscillation, dramatically decrease. This decrease is associated with reduced penetration of a jet-like mass transfer between the cavity and the shear layer region, which, in turn, is linked to the degree of coupling between the cavity fluctuations and shear layer oscillations.

Acknowledgments

The authors are grateful to the Office of Naval Research for support under Grant #N00014-01-1-0606], monitored by Dr Pat Purtell and Dr Ronald Joslin. Appreciation is also due to Dr Ted Farabee for his advice in this class of self-excited oscillations.

References

Blake, W.K., 1986. Mechanics of Flow-Induced Sound and Vibration, Vols. 1 and 2. Academic Press, Inc., New York.

Bruggeman, J.C., 1987. Flow-Induced Pulsations in Pipe Systems. Doctoral Dissertation, Technical University of Eindhoven.

Bruggeman, J.C., Hirschberg, A., van Dongen, M.E.H., Wijnands, A.P.J., Gorter, J., 1989. Flow induced pulsations in gas transport systems: analysis of the influence of closed side branches. ASME Journal of Fluids Engineering 111, 484–491.

Bruggeman, J.C., Hirschberg, A., van Dongen, M.E.H., Wijnands, A.P.J., Gorter, J., 1991. Self-sustained aero-acoustic pulsations in gas transport systems: experimental study of the influence of closed side branches. Journal of Sound and Vibration 150, 371–393.

Burroughs, C.B., Stinebring, D.R., 1994. Cavity flow tones in water. Journal of Acoustical Society of America 95, 1256–1263.

Bruggeman, J.C., Velekoop, J.C., Van Der Knapp, F.G.P., Keuning, P.J., 1991. Flow-excited resonance in a cavity covered by a grid: theory and experiments. NCA-11/FED-130, Flow Modeling, Measurement and Control ASME, pp. 135–144.

Cattafesta, L., Williams, D., Rowley, C., Alvi, F., 2003. Review of Active Control of Flow-Induced Cavity Resonance. AIAA Paper 2003–3567, 33rd AIAA Fluid Dynamics Conference, June 23–26, Orlando, FL, USA.

Celik, E., Rockwell, D., 2002. Shear layer oscillation along a perforated surface: a self-excited large-scale instability. Physics of Fluids 14 (12), 4444–4447.

Celik, E., Rockwell, D., 2004. Coupled oscillations of flow along a perforated plate. Physics of Fluids 16, 1714–1724.

Chomaz, J.M., Huerre, P., Redekopp, L.T., 1988. Bifurcations to local and global modes in spatially developing flows. Physics of Fluids Letters 60, 25–28.

Cremer, L., Ising, H., 1967/68. Die Selbsterregte Schwingungen von Orgelpfeifen. Acustica 19, 143–153.

Crighton, D.G., 1992. The jet-edge-tone feedback cycle: linear theory for the operating stages. Journal of Fluid Dynamics 1234, 361–392.

Cumpsty, N.S., Whitehead, D.S., 1971. The excitation of acoustic resonances by vortex shedding. Journal of Sound and Vibration 18 (3), 353–369.

Davies, P.O.A.L., 1981. Flow-acoustic coupling in ducts. Journal of Sound and Vibration 77 (2), 191–209.

Davies, P.O.A.L., 1996. Aeroacoustics and time varying systems. Journal of Sound and Vibration 190, 345–362.

DeMetz, F.C., Farabee, T.M., 1977. Laminar and turbulent Shear flow-induced resonances. AIAA Paper 77-1293.

Dequand, S., Hulshoff, S.J., Hirschberg, A., 2003. Self-sustained oscillations in a closed side branch system. Journal of Sound and Vibration 265 (2), 359–386.

Dequand, S., Luo, X., Willems, J., Hirschberg, A., 2003. Helmholtz-like resonator self-sustained oscillations, part 1: acoustical measurements and analytical models. AIAA Journal 41 (3), 408–415.

Dequand, S., Hulshoff, S., Van Kuijk, H., Willems, J., Hirschberg, A., 2003. Helmholtz-like resonator self-sustained oscillations, Part 2: detailed flow measurements and numerical simulations. AIAA Journal 41 (3), 416–423.

Dickey, N.S., Selamet, A., Ciray, M.S., 2001. An experimental study of the impedance of perforated plates with grazing flow. Journal of Acoustical Society of America 110, 2360–2370.

Ekmekci, A., Rockwell, D., 2003. Self-sustained oscillations of the shear flow past a slotted plate coupled with cavity resonance. Journal of Fluids and Structures 17 (8), 1237–1245.

Elder, S.A., 1978. Self-excited depth-mode resonance for a wall-mounted cavity in turbulent flow. Journal of Acoustical Society of America 64 (3), 877–890.

Flatau, A., Van Moorham, W.K., 1990. Prediction of vortex shedding responses in segmented solid rocket motors. AIAA Paper 90-2073.

Fletcher, N.H., 1979. Air flow and sound generation in musical wind instruments. Annual Review of Fluid Mechanics 11, 123–146.

Geveci, M., Oshkai, P., Rockwell, D., Lin, J.-C., Pollack, M., 2003. Imaging of the self-excited oscillation of flow past a cavity during generation of a flow tone. Journal of Fluid and Structures 18 (6), 665–694.

Gharib, M., Roshko, A., 1987. The effect of flow oscillations on cavity drag. Journal of Fluid Mechanics 117, 501–530.
Hofmans, G.C.J., 1998. Vortex sound in confined flows. Doctoral Dissertation, Technical University of Eindhoven, The Netherlands.
Hourigan, K., Welsh, M.C., Thompson, M.C., Stokes, A.N., 1990. Aerodynamic sources of acoustic resonance in a duct with baffles. Journal of Fluids and Structures 4, 345–370.
Howe, M.S., 1975. Contributions to the theory of aerodynamic sound with applications to excess jet noise and the theory of the flute. Journal of Fluid Mechanics 71 (4), 625–673.
Howe, M.S., 1980. The dissipation of sound at an edge. Journal of Sound and Vibration 70, 407–411.
Howe, M.S., 1997. Edge, cavity and aperture tones at very low mach numbers. Journal of Fluid Mechanics 330, 61–84.
Howe, M.S., 1998. Acoustics of Fluid-Structure Interaction. Cambridge University Press, Cambridge.
Huang, X.Y., Weaver, D.S., 1991. On the active control of shear layer oscillations across a cavity in the presence of pipeline acoustic resonance. Journal of Fluids and Structures 5, 207–219.
Jing, X., Sun, X., Wu, J., Meng, K., 2001. Effect of grazing flow on the acoustic impedance of an orifice. AIAA Journal 39, 1478–1484.
Kirby, R., Cummings, A., 1998. The impedance of perforated plates subjected to grazing gas flow and backed by porous media. Journal of Sound and Vibration 217, 619–636.
Knisely, C., Rockwell, D., 1982. Self-sustained low-frequency components in an impinging shear layer. Journal of Fluid Mechanics 116, 157–186.
Kuo, C.-H., Huang, S.-H., 2001. Influence of flow path modification on oscillation of cavity shear layer. Experiments in Fluids 31, 162–178.
Kriesels, P.C., Peters, M.C.A.M., Hirschberg, A., Wijnands, A.P.J., Iafrati, A., Riccardi, G., Piva, R., Bruggeman, J.C., 1995. High amplitude vortex-induced pulsations in a gas transport system. Journal of Sound and Vibration 184 (2), 343–368.
Kwon, Y.-P., 1998. Feedback mechanism of low-speed edgetones. Journal of the Acoustical Society of America 104, 2084–2089.
Looijmans, N.H., Bruggeman, J.C., 1997. Simple vortex models for vibration and noise caused by a flow over louvers in a cavity opening. In: Proceedings of Fluid-Structures International Aeroelasticity, Flow-Induced Vibration and Noise Symposium, vol. 1. ASME AD, 53-1, pp. 351–359.
Nelson, P.A., 1982. Noise generated by flow over perforated surfaces. Journal of Sound and Vibration 83 (1), 11–26.
Nelson, P.A., Halliwell, N.A., Doak, P.E., 1981. Fluid dynamics of a flow excited resonance. Part I: experiment. Journal of Sound and Vibration 78 (1), 15–38.
Nelson, P.A., Halliwell, N., Doak, P.E., 1983. Fluid dynamics of a flow excited resonance, Part II: flow acoustic interaction. The dissipation of sound at an edge. Journal of Sound and Vibration 91, 375–402.
Oshkai, P., Geveci, M., Rockwell, D., Pollack, M., 2004. Imaging of acoustically coupled oscillations due to flow past a shallow cavity: effect of cavity length scale. Journal of Fluids and Structures 20 (2), 277–308.
Ozalp, C., Pinarbasi, A., Rockwell, D., 2003. Self-excited oscillations of turbulent inflow along a perforated plate. Journal of Fluids and Structures 17, 955–970.
Parker, R., 1966. Resonance effects in wake shedding from parallel plates: some experimental observations. Journal of Sound and Vibration 4, 62–72.
Powell, A., 1961. On the edgetone. Journal of the Acoustical Society of America 33 (4), 395–409.
Rockwell, D., 1983. Oscillations of impinging shear layers. Invited lecture, 20th aerospace sciences meeting of AIAA, January, 1981, Orlando, FL; AIAA Paper 81-0047; also see AIAA Journal 21, 645–664.
Rockwell, D., 1998. Vortex-body interactions. Invited contribution to Annual Review of Fluid Mechanics 30, 199–229.
Rockwell, D., Lin, J.-C., Oshkai, P., Reiss, M., Pollack, M., 2003. Shallow cavity flow tone experiments: onset of locked-on states. Journal of Fluids and Structures 17 (3), 381–414.
Rockwell, D., Naudascher, E., 1978. Review—self-sustaining oscillations of flow past cavities. ASME Journal of Fluids Engineering 100, 152–165.
Rockwell, D., Naudascher, E., 1979. Self-sustained oscillations of impinging free-shear layers. Annual Review of Fluid Mechanics 11, 67–94.
Rockwell, D., Schachenmann, A., 1982. Self-generation of organized waves in an impinging turbulent jet at low mach numbers. Journal of Fluid Mechanics 117, 425–441.
Rockwell, D., Schachenmann, A., 1983. The organized shear layer due to oscillations of a turbulent jet through an axisymmetric cavity. Journal of Sound and Vibration 87 (3), 371–382.
Ronneberger, D., 1980. The dynamics of shearing flow over a cavity-a visual study related to the acoustic impedance of small orifices. Journal of Sound and Vibration 71, 565–581.
Rowley, C.W., Colonius, T., Basu, A.J., 2002. On self-sustained oscillations in two-dimensional compressible flow over rectangular cavities. Journal of Fluid Mechanics 455, 315–346.
Sever, C., Rockwell, D., 2005. Oscillations of shear flow along a slotted plate: small- and large-scale structures. Journal of Fluid Mechanics 530, 213–222.
Stoneman, S.A.T., Hourigan, K., Stokes, A.N., Welsh, M.E., 1988. Resonant sound caused by flow past two plates in tandem in a duct. Journal of Fluid Mechanics 192, 455–484.
Tsui, C.Y., Flandro, G.A., 1977. Self-induced sound generation by flow over perforated duct liners. Journal of Sound and Vibration 50, 315–331.

Ziada, S., 1999. Feedback control of flow-excited cavity resonance. ASME Pressure Vessels & Piping Division, PVP 389, p. 325.
Ziada, S., Bühlmann, E.T., 1992. Self-excited resonances of two-side-branches in close proximity. Journal of Fluids and Structures 6, 583–601.
Zoccola, P.J., 2002. Excitation by flow over an obstructed opening. ASME Applied Mechanics Division AMD 253 (2), 899–906.
Zoccola, P.J., 2004. Effect of opening obstructions on the flow-excited response of a Helmholtz resonator. Journal of Fluids and Structures 19 (7), 1005–1025.